Quantifying nitrogen fixation by heterotrophic bacteria in sinking marine particles

Subhendu Chakraborty (schakraborty@bio.ku.dk)
University of Copenhagen https://orcid.org/0000-0002-2904-9313
Ken Andersen
Technical University of Denmark https://orcid.org/0000-0002-8478-3430
Andre Visser
Danish Fisheries https://orcid.org/0000-0002-1604-7263
Keisuke Inomura
University of Washington
Michael J. Follows
Massachusetts Institute of Technology (MIT)
Lasse Riemann
University of Copenhagen https://orcid.org/0000-0001-9207-2543

Article

Keywords: N2 fixation, Sinking marine particles, Heterotrophic bacteria, Anaerobic respiration, Anoxic 35 interior, Trait-based optimization model

Posted Date: November 14th, 2020

DOI: https://doi.org/10.21203/rs.3.rs-103042/v1

Version of Record: A version of this preprint was published at Nature Communications on July 2nd, 2021.
See the published version at https://doi.org/10.1038/s41467-021-23875-6.

Quantifying nitrogen fixation by heterotrophic bacteria in sinking marine particles

Subhendu Chakraborty[1,2,*], Ken H. Andersen[2], André W. Visser[2], Keisuke Inomura[3], Michael J. Follows[4], Lasse Riemann[1,*]

[1]*Department of Biology, Marine Biological Section, University of Copenhagen, Helsingør, Denmark*

[2]*Centre for Ocean Life, DTU Aqua, Technical University of Denmark, Kemitorvet, 2800 Kgs. Lyngby, Denmark*

[3]*School of Oceanography, University of Washington, Seattle, WA, USA*

[4]*Department of Earth, Atmosphere and Planetary Sciences, MIT, Cambridge, MA, United States of America*

Running title: Nitrogen fixation in sinking marine Particles

*Corresponding authors: Department of Biology, Marine Biological Section, University of Copenhagen, Helsingør, Denmark. Tel: +4591714664. Email: schakraborty@bio.ku.dk; lriemann@bio.ku.dk

Abstract

Nitrogen (N_2) fixation by heterotrophic bacteria associated with sinking particles contributes to marine N cycling, but a mechanistic understanding of its regulation and significance are not available. Here we develop a mathematical model for unicellular heterotrophic bacteria growing on sinking marine particles and can fix N_2 under suitable environmental conditions. We find that the interactive effects of polysaccharide and polypeptide concentrations, sinking speed of particles, and surrounding O_2 and NO_3^- concentrations determine the N_2 fixation rate inside particles. N_2 fixation inside sinking particles is mainly fueled by SO_4^{2-} respiration rather than NO_3^- respiration. Our model suggests that anaerobic processes, including heterotrophic N_2 fixation, can take place in anoxic microenvironments inside sinking particles even in fully oxygenated marine waters. The modelled rates are similar to bulk rates measured in the aphotic ocean, and our study consequently suggests that particle-associated heterotrophic N_2 fixation contributes significantly to oceanic N_2 fixation.

Keywords

N_2 fixation; Sinking marine particles; Heterotrophic bacteria; Anaerobic respiration; Anoxic interior; Trait-based optimization model

Introduction

Nitrogen (N) is an essential element for all living organisms but its availability often limits the growth and productivity of terrestrial and aquatic ecosystems. Although molecular dinitrogen gas (N_2) is highly abundant in the marine water column, only specific prokaryotes that can fix N_2 (diazotrophs) using the nitrogenase enzyme complex[1] assimilate this form of nitrogen. Nevertheless, nitrogen fixation maintains the inventory of biologically available nitrogen in the open oceans, which fuels primary production[1,2], and thereby affects the biogeochemical cycling of both nitrogen and carbon[3].

N_2 fixation was thought to exclusively be carried out by cyanobacteria in the oligotrophic and sunlit upper layers of the tropical and subtropical oceans (reviewed in Zehr[4]). However, accumulating evidence shows that N_2 fixation is surprisingly widespread, for example in the deep sea[5], nutrient-rich coastal waters[6], and cold Arctic waters[7]. Moreover, analyses of genes (*nifH*) encoding the enzyme complex used for N_2 fixation document that non-cyanobacterial diazotrophs are almost ubiquitous across the world's oceans, often dominate *nifH* gene libraries over cyanobacteria, and occasionally express nitrogenase[8–10]. Hence, the emerging picture shows N_2 fixation as a global marine process partially carried out by non-cyanobacterial diazotrophs, but their ecology and contribution to total N_2 fixation remain enigmatic[10].

Nitrogenase is irreversibly inactivated by O_2[11]. Cyanobacteria adopt several strategies to protect nitrogenase from inactivation by O_2[12]. Heterotrophic diazotrophs may under rich culture conditions surround cells with extracellular polymers[13] to lower the permeability to extracellular O_2 to protect the nitrogenase, but since this is highly energy-demanding[14] it is an unlikely strategy in the relatively nutrient-poor marine water column. Recent work, inspired by the pioneering work of Paerl and co-workers[15,16], has suggested that heterotrophic N_2 fixation takes place in low-oxygen or

anaerobic microzones associated with marine particles (reviewed in Riemann et al.[17] and in Bombar et al.[10]). Indeed, anaerobic microzones are occasionally associated with marine particles[18,19]. Recent studies show N_2 fixation is stimulated by the presence of particles[20,21] and that heterotrophic diazotrophs are associated with plankton specimens[22,23] and marine aggregates[24,25]. Hence, beyond doubt, marine particles provide, at least ephemeral, conditions suitable for N_2 fixation by heterotrophic bacteria.

Cellular O_2 removal by diazotrophs is considered highly energy-demanding, even more energetically expensive than N_2 fixation *per se*[14]. Hence, considerable amounts of labile carbon (e.g. carbohydrate and amino acids) are required to sustain particle-associated microbial respiration beyond the specific energy requirements for diazotrophy. Interestingly, preferential microbial utilization of N-rich organics on particles[26] and release of NH_4^+ [27] may increase particle C:N ratios over time[26], gradually making N acquisition by N_2 fixation increasingly advantageous.

While synthesizing ATP during respiration, O_2 is used as the most common and favorable form of electron acceptor by prokaryotes. In the absence of O_2, other electron acceptors (e.g. NO_3^- and SO_4^{2-}) may be used in a stepwise manner according to their free energy yields[28], with a rather small drop-off in the theoretical energy yield for NO_3^- respiration, followed by SO_4^{2-} respiration with almost tenfold less energy yield per electron donor[29]. However, SO_4^{2-} respiration is likely the primary form of anaerobic respiration supporting N_2 fixation since SO_4^{2-} reducing diazotrophs have been widely found[30,31], also on marine particles[32,33].

Another important factor regulating N_2 fixation in sinking marine particles is the particle size, which varies from micrometers to several millimeters[34]. The particle size spectrum follows a power law relationship showing a decrease in particle abundance with increasing size[35]. Because of smaller surface to volume ratios, large particles are more likely to develop an anoxic interior

suitable for N_2 fixation. Moreover, particles face changing O_2 and NO_3^- concentrations while descending in the water column. The rate of change depends on particle sinking speed, but no universal size-sinking speed relationship exists[36]. Although all these external factors can have huge influences, the extent by which they affect heterotrophic N_2 fixation inside sinking particles is currently unclear.

To quantitatively analyze the conditions when heterotrophic N_2 fixation occurs on sinking particles, we present a trait-based model of heterotrophic bacteria associated with sinking particles. This effort aims to encapsulate an understanding of the dynamics between (micro)environmental conditions and the requirements and constraints of heterotrophic N_2 fixation. Specifically, the model captures basic cellular processes determining growth and N_2 fixation in an individual cell, and then scales up to the population level to address particle dynamics and the contribution to total N_2 fixation in the water column. We also examine how the size of particles, initial concentrations of polysaccharide and polypeptide, and environmental O_2 concentration influence heterotrophic N_2 fixation inside sinking particles, and the succession of aerobic and anaerobic respiration as support for N_2 fixation. In doing so we identify potentially testable hypothetical consequences: (H1) Excess acquired N released by cells and hydrolysis products diffuse away from the particle and contribute to an organic solute trail in the water column as the particle sinks. (H2) N_2 fixation by heterotrophic diazotrophs depends on the generation of particle-associated low-oxygen microenvironments. (H3) During the "life span" of a sinking marine particle there is an ephemeral window of opportunity where environmental conditions are conducive for heterotrophic N_2 fixation. (H4) SO_4^{2-} reduction is more important for N_2 fixation within sinking particles than NO_3^- reduction. (H5) The particle sinking speed and concentrations of O_2 and NO_3^- in the water column affects N_2 fixation rates. Although the model is developed to investigate N_2 fixation, it also provides critical insights on biochemistry and microbial respiratory processes inside sinking particles.

Results and discussion

Overview of the model

The overall model consists of a 'cell model' and a 'particle model'. The cell model describes basic cellular processes, like uptake of resources, respiration, growth, and N_2 fixation rate. The cell model is embedded in a dynamic model, called 'the particle model', that deals with interactions of cells with the available abiotic factors (polysaccharide, polypeptide, O_2, NO_3^-, SO_4^{2-}) over time.

The cell model: The model describes a population of facultative N_2 fixing heterotrophic bacteria growing inside a particle sinking through a water column. A schematic representation of the processes inside a single cell is presented in Figure 1 and the full description of mathematical forms and equations are provided in the Methods section. The cell uses ectoenzymes to degrade polymers (polysaccharides and polypeptides) to oligomers or monomers (glucose and amino acids) that it can efficiently take up to fulfill its C and N requirements. The uptake of glucose and amino acids follows Michaelis-Menten kinetics. The model accounts for acquired C and N to ensure that the cell satisfies its needs for both. While glucose uptake provides only C, amino acids provide both C and N (equations (1) and (2)).

C obtained from glucose and amino acids is respired to carry out resource uptake, cellular maintenance (Fig. 1), and standard metabolism (equation (6)). O_2, NO_3^-, and SO_4^{2-} are used as electron acceptors in a stepwise manner in order of their free energy yield to perform respiration[37]. In the absence of sufficient O_2, the cell uses NO_3^- to continue respiration, although all N necessary for growth comes from organic sources and N_2 fixation (whenever possible). The further need of electron acceptor is fulfilled by SO_4^{2-}.

The cell can carry out N_2 fixation to supplement its N requirement. It regulates the rate of N_2 fixation to optimize its growth rate. As nitrogenase is irreversibly inhibited by O_2[11], the cell needs low O_2 conditions inside particles or increased respiration to make the cell O_2 free and thereby enable N_2 fixation.

The synthesis of biomass using available C and N from resource uptake and electron acceptors follows Liebig's law of the minimum and is constrained by the cellular C:N ratio ($\rho_{\mathrm{CN,B}}$) (equation (21)). Any excess assimilated C or N is excreted from the cell. The cell division rate μ is found from the mass-specific synthesis rate.

The particle model: We consider a sinking particle consisting of polysaccharides and polypeptides and colonized by facultative nitrogen-fixing bacteria (Supplementary Fig. S1). Only fractions of these polymers are considered labile, i.e. accessible by bacteria. Bacterial enzymatic hydrolysis converts labile polysaccharides and polypeptides into monosaccharides (glucose) and amino acids that are efficiently taken up by bacteria. Excess glucose and amino acids diffuse out of the particle to the surrounding environment, while O_2 and NO_3^- diffuse into the particle from the surrounding water. Due to high concentrations of SO_4^{2-} and N_2 in ocean waters[38,39], these elements are assumed not to be diffusion-limited inside particles, their uptakes are, therefore, limited by the cellular maximum uptake capacities. Depending on the concentrations of glucose, amino acids, O_2, NO_3^-, and SO_4^{2-} inside the particle, bacteria carry out N_2 fixation (equation (23)). Fe, an essential component in the nitrogenase complex, is considered nonlimiting as sinking particles contain high levels of Fe[40]. The interactions between particle, cells, and the surrounding environment are explained in Fig. S1, equations are provided in Table 1, and a full description of the particle model is provided in the Methods section.

Biochemical dynamics inside a particle under static environmental conditions

The dynamics inside a particle of radius 0.125 cm with initial polysaccharide and polypeptide concentrations of 2.6×10^8 µg G L^{-1} and 1.6×10^8 µg A L^{-1}, with relative lability of 0.238 and 0.5, respectively, are depicted in Fig. 2. We simulate a population of bacterial cells of radius 0.29 µm (50 fg C $cell^{-1}$) growing inside a particle where the surrounding glucose, amino acids, O_2, NO_3^-, and SO_4^{2-} concentrations are kept fixed at 50 µg G L^{-1}, 5 µg A L^{-1}, 50 µmol O_2 L^{-1}, 15 µmol NO_3 L^{-1}, and 29×10^3 µmol SO_4 L^{-1}. Here, concentrations inside the particle are given as per liter of particle and outside as per liter of water. A full description of the included parameters and their values is available in Supplementary Material S1 and Table S1. The bacteria hydrolyze labile polysaccharides and polypeptides into glucose and amino acids using ectoenzymes (Fig. 2a, b). As a result, glucose and amino acid concentrations increase (Fig. 2c, d), which causes a high growth rate of cells (~3.6 d^{-1}; Fig. 2j), an increase in bacterial abundance (Fig. 2g), and a decrease in labile polysaccharide and polypeptide concentrations. The occurrence of such high growth rate[41] and bacterial abundance[25,42,43] is not seldom inside natural sinking particles. The increased community respiration (Fig. 2h) decreases O_2 concentration and eventually leads to anoxia in the particle interior (Fig. 2e). This is consistent with ephemeral anoxia inside marine aggregates[19] and the anoxia observed inside suspended cyanobacterial colonies of comparable size[18]. The gradual formation of low-oxygen or anoxic conditions and depletion of organic N (amino acids) facilitates N_2 fixation (Fig. 2i), supported by aerobic respiration followed by NO_3^- respiration (Fig. 2e, f). The lesser energetic yield of NO_3^- respiration leads to a reduced growth rate (~0.6 d^{-1}). Furthermore, when NO_3^- becomes exhausted (Fig. 2f), cells respire SO_4^{2-} (not shown in the figure) and the growth rate becomes very low (~0.2 d^{-1}). Because of the energetic constraints, N_2 fixation during this phase becomes low and eventually ceases due to increased O_2 levels as the exhaustion of labile

carbon in the particle decreases cell concentration and O_2 influx exceeds O_2 consumption (aerobic respiration).

Cellular mechanisms of N_2 fixation

To explore the cellular mechanism of N_2 fixation, we examine concentrations and rates over time at a radial distance of 0.027 cm from the particle center (Fig. 3). We identify four phases based on limitations of either C or N or electron acceptor where the growth rate is determined by the minimum availability of these three substances (equations (21) and (22); Fig. 3a). Available C for growth is the C remaining from total C uptake after paying the respiratory costs, whereas the N available for growth comes from uptake and N_2 fixation.

I (C limited phase): Cells are limited by C, which is seen by the light blue line coinciding with the magenta line in Fig. 3a. Growth rates are high, up to 3.6 day^{-1}. Excess N and hydrolysis products not taken up by cells[26] will diffuse away from the particle and contribute to an organic solute trail in the water column as the particle sinks[44], supporting our hypothesis H1.

II (High respiration phase): The large bacterial population causes high community respiration, matching or exceeding the diffusive influx of O_2, and anoxia forms in the particle interior (Fig. 3e). Cells start respiring NO_3^- and even SO_4^{2-} reduction happens at the end of this phase (not shown in the figure) when NO_3^- is depleted. Now growth is limited by the availability of electron acceptor (the yellow line coincides with the magenta in Fig. 3a). An organic solute trail rich in both C and N is predicted during this phase. The amino acid concentration decreases rapidly during the final part of this phase (Fig. 3c).

III (N_2 fixing phase): Because of our initial choice of polysaccharide and polypeptide concentrations, amino acids are exhausted. In real life, bacterial preferential degradation of N-rich organics results in similar early exhaustion of amino acids[26]. Glucose remains available as C source (Fig. 3c), so cells start fixing N_2 to maintain growth (Fig. 3d). However, since the available O_2 in the particle is insufficient to support respiration, NO_3^- and SO_4^{2-} also act as electron acceptors during this phase. Cells become co-limited by N from N_2 fixation and electron acceptor (green and yellow lines coincide; Fig. 3a) and we predict that the expected solute trail consists only of C during this phase. Because of the lower free energy yield, N_2 fixation decreases when using SO_4^{2-} as an additional electron acceptor. Towards the end of this phase, the respiratory cost of glucose uptake decreases with the decrease in glucose concentration to such an extent that there is excess O_2 after performing respiration. At that point, cells increase respiration to burn excess O_2 to perform N_2 fixation for a very short interval of time, resulting in a peak in N_2 fixation rate (Fig. 3d) and the respiratory cost for O_2 removal (Fig. 3b).

IV (Fading phase): Cells have insufficient C to deal with excess O_2 and consequently stop N_2 fixation. N becomes the limiting factor for cell growth and growth ceases. Later, the growth rate becomes negative as there is no glucose left needed for basal respiration. Throughout this phase, the bacterial concentration decreases (Fig. 3c).

Comparing different respiratory costs related to N_2 fixation in terms of direct respiration, enzyme production, and O_2 removal, it becomes evident that when cells use respiratory protection to keep nitrogenase viable and enable N_2 fixation, the related cost becomes much higher than the direct cost for N_2 fixation (Fig. 3b). A similar high cost of O_2 management during N_2 fixation was previously shown to exceed the costs of N_2 fixation *per se* for the heterotrophic soil bacterium *Azotobacter vinelandii*[14]. We therefore conclude that active O_2 management by particle-associated

heterotrophic diazotrophs is not prevalent, but that they rather depend on the generation of low-oxygen microenvironments by community respiration, supporting our initial hypothesis H2.

Effects of particle size, O_2, and initial polysaccharide and polypeptide concentrations

Marine particles are highly variable in size[34] and chemical composition. For example, the C:N ratio (and implied polysaccharide:polypeptide availability) varies considerably, depending on environmental conditions[45]. Moreover, while descending in the water column, particles face a range of surrounding O_2 concentrations. Therefore, we examined the implications for N_2 fixation in particles of different sizes under different polysaccharide, polypeptide, and O_2 concentrations (Fig. 4). We considered open ocean particles with radius 5 μm to 0.25 cm[46] and estimated the total amount of fixed N_2 per particle by allowing bacteria to grow inside particles for 20 days. As expected, large particles provide a suitable environment for N_2 fixation. The minimum size of particles where N_2 fixation is possible increases with polysaccharide concentration (Fig. 4a), decreases with environmental O_2 concentration (Fig. 4c), and attains a maximum at intermediate polypeptide concentration (Fig. 4b). N_2 fixation does not occur in particles with radius below ~0.03 cm. The increase in N_2 fixation with polysaccharide concentrations is consistent with observations of stimulated N_2 fixation in seawater upon the addition of C substrate (e.g. Rahav et al.[21]). Interestingly, maximum N_2 fixation occurs at intermediate polypeptide concentrations (~5×10^7 μg L^{-1}) in large particles (Fig. 4b). Our interpretation is that low polypeptide concentrations do not allow cells to grow to high concentrations and create an anoxic interior, whereas, at high concentrations, cells cover their N demand by amino acid assimilation and, therefore, refrain from N_2 fixation.

Maximum N_2 fixation in large particles occurs under very low (~0.3 μmol L^{-1}) and intermediate (~80 μmol L^{-1}) O_2 levels (Fig. 4c). Under very low O_2 concentrations, cellular respiration is expected to occur using NO_3^- and SO_4^{2-} as electron acceptors causing low cellular growth rate and a slowly increasing cell concentration. However, N_2 fixation occurs for a long time period and makes the total N_2 fixation per particle relatively high (Supplementary Fig. S2d). At intermediate O_2 levels, cells are not limited by O_2 and reach a high growth rate during the initial phase. Therefore a high cell concentration is rapidly obtained (Supplementary Fig S2c) causing reduced O_2 levels suitable for N_2 fixation for a relatively shorter time interval (Supplementary Fig S2d). The combination of high cellular N_2 fixation rate and high cell concentration results in high total N_2 fixation per particle. At a high O_2 level (~200 μmol L^{-1}), this low O_2 period is very short, possibly because of a large diffusion loss of glucose associated with extensive polysaccharide hydrolysis caused by the high cell concentration (Supplementary Fig S2c). This lowers the total amount of N_2 fixed per particle. However, the concentrations of O_2, where these two maxima occur, depend on the initial polysaccharide and polypeptide concentrations. With a decrease in these concentrations, the intermediate O_2 concentration, where the maximum occurs, decreases (Supplementary Fig. S3) and finally merges with the other maximum at low O_2 (not shown). Indeed, empirical results confirm the existence of such optimal O_2 concentration for N_2 fixation and a level of 6 μmol L^{-1} has been observed for heterotrophic diazotrophs[47].

By simultaneously varying initial labile polysaccharide and polypeptide concentrations in small and large particles at different surrounding O_2 concentrations, it appears that N_2 fixation is restricted to large particles with high initial polysaccharide and polypeptide concentrations when O_2 concentration is high (Fig. 5a). However, under low O_2 concentrations, N_2 fixation occurs even at lower concentrations of polysaccharides and polypeptides (Fig. 5b). N_2 fixation can also occur in

267 relatively smaller particles, however, only when the initial polysaccharide concentration is high and
268 the surrounding O_2 concentration is low (Fig. 5c).

269 The amount of POC present in particles can be considered a proxy for polysaccharide and
270 polypeptide concentrations. The presence of high POC in freshly formed particles from dense
271 phytoplankton blooms[48] and fecal pellets[49] would increase the likelihood of particle-associated N_2
272 fixation. Likewise, the seasonally high POC content of particles during late spring in high latitude
273 areas[50] could increase the likelihood of particle-associated N_2 fixation at this time. On the other
274 hand, the size of particles, which also has a profound impact on N_2 fixation, is closely associated
275 with the species responsible for particle formation. For instance, since particles are larger during
276 diatom blooms compared to cyanobacterial blooms[51], an increased likelihood of N_2 fixation during
277 diatom blooms would be expected. The latitudinal variation in particle size spectrum with a
278 dominance of larger particles at higher latitudes compared to smaller particles in the oligotrophic
279 subtropical gyres [52] indicates a greater opportunity for particle-associated N_2 fixation at high
280 latitudes. Hence, the potential for particle-associated N_2 fixation is highly dependent on local
281 dynamics in the size and composition of particles, together with the local O_2 conditions.

282

283 *N_2 fixation in sinking particles*

284 To explore the dynamics of N_2 fixation in sinking particles of different sizes, we use vertical
285 profiles of O_2 and NO_3^- in the upper 500 m of the Mauritanian upwelling zone in the North
286 Atlantic Ocean (NAO; Fig. 6)[53]. O_2 concentration drops to hypoxic levels (~62.5–157 µmol L^{-1}) in
287 the water column between 100–600 m (Fig. 6a). N_2 fixation coincides mainly with the presence of
288 an anoxic particle interior. The amount of fixed N_2 increases with particle size and because of
289 higher sinking rates and more C to fuel respiration the existence of both anoxic interior (regions

within magenta lines) and N_2 fixation (within white lines) in large particles occur in deeper waters and persist for longer time (Fig. 6b). We presume that N_2 fixation stops in deep water when labile material in the particle is exhausted. This shows that the window of opportunity where environmental conditions are conducive for heterotrophic N_2 fixation is ephemeral, supporting our hypothesis H3.

In the anoxic particle interior, NO_3^- and SO_4^{2-} function as electron acceptors. The model suggests that the fraction of particle volume where denitrification occurs (maximum 6%) is much smaller than the fraction of volume of occurrence of SO_4^{2-} reduction (maximum 90%) (Fig. 6c, d). The model predicts that despite being energetically profitable, NO_3^- does not play a big role in N_2 fixation and SO_4^{2-} reduction appears as the key anaerobic process within sinking particles. This is due to very high cell concentration near the surface of the particle (Fig. 2g) that creates a high respiratory demand for electron acceptors, exhausts NO_3^- close to the particle surface, and prevents NO_3^- from reaching the particle interior (Fig. 2f). As a result, N_2 fixation in most of the particle interior is supported by SO_4^{2-} respiration, which confirms the importance of SO_4^{2-} reduction in particle-associated N_2 fixation compared to NO_3^- reduction, supporting hypothesis H4. Diazotrophy among SO_4^{2-} reducing bacteria is well established in various marine environments[54,55].

Influence of sinking speed on particle-based N_2 fixation.

The speed at which particles sink is a critical parameter since it determines the duration of exposure to environmental conditions (e.g. O_2) that influence N_2 fixation inside particles. Sinking speed is affected by a multitude of factors related to particle composition, size, and density[56–58], and no

312 universal size-sinking velocity relationship exists[36]. We, therefore, examine scenarios with three
313 types of particles: (1) natural marine snow measured *in situ* off California[59], (2) laboratory-made
314 diatom aggregates and (3) coccolithophore aggregates measured *in vitro*[48]. Sinking speed is lowest
315 for natural marine snow followed by diatom aggregates and coccolithophore aggregates (Fig. 7a).
316 For the sake of simplicity, these particles are assumed to vary only in their sinking speeds and not in
317 their initial concentrations and lability of polysaccharides and polypeptides. We again use the
318 vertical profile of O_2 and NO_3^- at the NAO but extended to 1,500 m depth with a hypoxic region
319 between 100-600 m depth (Fig. 7b).

320 Three different aspects are evident from the analysis. Firstly, when particles sink at a speed
321 similar to natural marine snow (~15-75 m d^{-1}), anoxic microenvironments are created (regions
322 within magenta lines) and N_2 fixation happens (indicated by color) in particles within the hypoxic
323 zone (Fig. 7e). However, with higher sinking speeds similar to diatom (~2-180 m d^{-1}) and
324 coccolithophore (~20-375 m d^{-1}) aggregates, the existence of anoxia and N_2 fixation inside particles
325 can extend beyond the hypoxic strata of the water column (Fig. 7d,e); both anoxic interior and N_2
326 fixation are predicted even at 1,800 m depth for large coccolithophore aggregates (not in the figure).
327 Secondly, the depth window where N_2 fixation occurs increases with particle sinking speed (7c-e).
328 Finally, our study predicts that the highest N_2 fixation rate (1.46 μg N (cm^3 particle)$^{-1}$ d^{-1}) is attained
329 in large particles at intermediate sinking velocities, similar to that of diatom aggregates (Fig. 7d).
330 Since, NO_3^- respiration yields more energy than SO_4^{2-} reduction, we speculate that the presence of
331 relatively higher concentrations of NO_3^- during the time of N_2 fixation helps to boost N_2 fixation
332 rate in diatom aggregates. High sinking speed, similar to that of coccolithophore aggregates,
333 transports particles quickly to deep water with high NO_3^- and O_2 concentrations (Fig. 7e). We
334 expect that high NO_3^- concentration favors relatively high N_2 fixation, but high O_2 concentration
335 decreases the N_2 fixation rate in coccolithophore aggregates. Therefore, the interplay between

particle sinking speed and vertical water column profiles of O_2 and NO_3^- concentrations determines the N_2 fixation rate, supporting our hypothesis H5.

N_2 fixation in contrasting oceanic environments

N_2 fixation is dependent on the O_2 and NO_3^- concentrations in the water column, but those are highly variable around the global ocean. We investigated N_2 fixation rates in three contrasting water columns: an O_2 minimum zone in the Eastern Tropical South Pacific (ETSP)[53], the Mauritanian upwelling zone in the NAO[53], and an open ocean site (OO; 30.5°N, 52.5°W)[60,61]. The ETSP has O_2 minimum zones with < 5 µmol O_2 L^{-1} at ~150–600 m depth (Fig. 8a), the NAO has reduced O_2 levels (~62.5–157 µmol L^{-1}) at ~100–600 m (Fig. 8d), whereas the open ocean site has high O_2 concentration throughout the water column (>157 µmol L^{-1}; Fig. 8g). NO_3 concentrations increase gradually up to 800 m depth, with decreasing levels from ETSP to NAO and to the open ocean site. We consider particles with sinking speed similar to natural marine snow and examine N_2 fixation rates per unit volume of particle (fig 8c,f,i). To compare with existing measurements, we further calculate N_2 fixation rates per unit volume of water (Fig. 8b,e,h) and depth-integrated N_2 fixation rates by multiplying the number of particles with N_2 fixation per particle (equation (34))[35].

Maximum N_2 fixation rates per volume of particle and per volume of water lie within ranges 0.31-1.1 µg N (cm^3 particle)$^{-1}$ d^{-1} (Fig. 8c,f,i) and 0.14-0.7 µmol N m^{-3} d^{-1} (Fig. 8b,e,h). The highest rate of N_2 fixation is in the NAO followed by the ETSP. Interestingly, N_2 fixation is observed even at the high O_2 concentrations of the open ocean, although, the N_2 fixation rates and the depth window of N_2 fixation are smaller than for the other two scenarios. Since the abundance and size spectrum of particles vary with latitude and seasonally at high latitudes[62], we test the sensitivity of N_2 fixation rates by varying the parameter determining the abundance (n_0) and the proportion of

large and small particles (ξ). We find that the N_2 fixation rate varies between 0.3-1.7 μmol N m^{-3} d^{-1} (Supplementary fig. S4). Our modelled N_2 fixation rates are comparable with bulk N_2 fixation rates measured in the aphotic ocean (0-0.89 μmol N m^{-3} d^{-1})[9,63] where active autotrophic cyanobacterial diazotrophs are not expected. Our calculated depth-integrated N_2 fixation rates lie within the range 7.1-65.1 μmol N m^{-2} d^{-1}. Empirical evidence from regions, where N_2 fixation is dominated by heterotrophic bacteria, show similar levels of depth-integrated N_2 fixation rates; e.g. 6.27–16.6 μmol N m^{-2} d^{-1} in the equatorial and southern Indian Ocean[64] and 12.4 – 190.9 μmol N m^{-2} d^{-1} in the South Pacific Gyre[65]. In comparison, depth-integrated N_2 fixation rates by cyanobacteria in most regions of the global upper ocean are in the order of 1–100 μmol N m^{-2} d^{-1} [66]. Hence, taken together, our modelled rates for heterotrophic bacteria on particles are consistent with empirical bulk rates from the deep sea and comparable to areal rates measured for cyanobacteria. This supports empirical studies suggesting that aphotic fixation can account for a significant or even predominant fraction of water column N_2 fixation[63,67], and substantiates the idea that aphotic N_2 fixation may be important to global nitrogen budget considerations[5].

Conclusions and broader implications

Our model suggests that particle-associated heterotrophic N_2 fixation is viable and reasonable based on the known properties and physics of marine particles and reveals a significant contribution to the oceanic biological N_2 fixation. The likelihood and rate of N_2 fixation associated with any individual particle will depend upon numerous factors including the initial polysaccharide and polypeptide concentrations (and associated C:N ratio), the size and sinking speed of the particle, and the vertical profiles of O_2 and NO_3^- through which the particle sinks. We show how low-O_2 or anoxic zones generated inside sinking particles by microbial respiration provide conditions suitable for

heterotrophic N_2 fixation, however, only in particles larger than about 0.03 cm. Moreover, we show that these anoxic microenvironments can promote anaerobic respiratory processes that even extend into well-oxygenated deep waters. Interestingly, our simulations suggest that even in particles that favor N_2 fixation at a point in their descent, the window of time (depth) where diazotrophy occurs is likely to be short. However, despite the necessity of several coinciding environmental conditions for N_2 fixation in particles, the criteria are met in natural particles. Because of the huge number and heterogeneity among particles sinking in the ocean[68], it is highly likely that a large number of individual particles at any given time might meet these criteria and in doing so, confer a fitness advantage on a subset of bacteria that retain the ability to fix nitrogen. This may explain the ubiquity and persistence of the genetic signature for heterotrophic N_2 fixation throughout the oceans[8]. The combined knowledge of the probability density of particle sizes, compositions, and sinking speeds is suggested to predict the average rates of N_2 fixation associated with particles.

Our model makes several interesting and potentially testable predictions: Firstly, the C:N composition of particle "trails" will reflect the interior state and might be a way to probe the response of different particle types or conditions. Secondly, the model predicts a "preference" for SO_4^{2-} electron acceptor over nitrate in low oxygen particles. Thirdly, heterotrophic diazotrophs mostly use local and ephemeral oxygen conditions and get windows of opportunity for their N_2 fixation. Fourthly, N_2 fixation can occur on large particles with high concentrations of polysaccharides and polypeptides in fully oxygenated marine waters, but also on older less substrate-rich particles if oxygen concentration in the surrounding water is low. These predictions could be promoted as perspectives for future experiments.

Methods

The cell model

Growth rate of a cell:

The growth rate of a bacteria cell depends on the acquisition of C (from the particle) and N (from the particle and through N_2 fixation), as well as on metabolic expenses in terms of C.

Uptake of C and N

Bacteria get C from glucose and both C and N from amino acids. The total amount of C available for the cell from monomers is (units of C per time)

$$J_{\mathrm{DOC}} = f_{\mathrm{G},C} J_G + f_{A,C} J_A, \quad (1)$$

and the amount of N available from monomer is (N per time)

$$J_{\mathrm{DON}} = f_{A,N} J_A, \quad (2)$$

where J_G and J_A are uptake rates of glucose and amino acids, $f_{\mathrm{G},C}$ is the fraction of C in glucose, and $f_{A,C}$ and $f_{A,N}$ are fractions of C and N in amino acids.

The rate of obtaining N through N_2 fixation is:

$$J_{N_2}(\psi) = \psi M_{N_2}, \quad (3)$$

where ψ $(0 < \psi < 1)$ regulates N_2 fixation rate and fixation can happen at a maximum rate M_{N_2}. N_2 fixation is only limited by the maximum N_2 fixation rate as dissolved dinitrogen (N_2) gas in seawater is assumed to be unlimited[39].

The total uptake of C and N from different sources becomes

$$J_C = J_{\mathrm{DOC}} \quad (4)$$

$$J_N(\psi) = J_{\mathrm{DON}} + J_{N_2}(\psi). \quad (5)$$

Costs

Respiratory costs of cellular processes together with N_2 fixation and its associated O_2 removal cost depend on the cellular O_2 concentration. Two possible scenarios can be observed:

Case 1: When O_2 concentration is sufficient to maintain aerobic respiration

Respiratory costs for bacterial cellular maintenance can be divided into two parts: one dependent on limiting substrates and the other one is independent of substrate concentration[69]. Here we consider only the basal respiratory cost $R_B x_B$, which is independent of the limiting substrates and is assumed as proportional to the mass of the cell x_B (µg C). In order to solubilize particles, particle-attached bacteria produce ectoenzymes that cleave bonds to make molecules small enough to be transported across the bacterial cell membrane. Cleavage is represented by a biomass-specific ectoenzyme production cost R_E[70]. The metabolic costs associated with the uptake of hydrolysis products and intracellular processing are assumed to be proportional to the uptake (J_i): $R_{\mathrm{G}} J_{\mathrm{G}}$ and $R_{\mathrm{A}} J_{\mathrm{A}}$ where the R_i's are costs per unit of resource uptake. In a similar way, the metabolic cost of N_2 fixation is assumed as proportional to the N_2 fixation rate: $R_{N_2}\rho_{\mathrm{CN,B}} J_{N_2}$, where $\rho_{\mathrm{CN,B}}$ is the bacterial C:N ratio. If we define all the above costs as direct costs, then the total direct respiratory cost becomes

$$R_{\mathrm{D}}(\psi) = R_B x_{\mathrm{B}} + R_E x_{\mathrm{B}} + R_{\mathrm{G}} J_{\mathrm{G}} + R_{\mathrm{A}} J_{\mathrm{A}} + R_{N_2}\rho_{\mathrm{CN,B}} J_{N_2}(\psi). \quad (6)$$

Indirect costs related to N_2 fixation arises from the removal of O_2 from the cell and the production/replenishment of nitrogenase as the enzyme is damaged by O_2. The cell can remove O_2 either by increasing respiration[71] or by increasing the production of nitrogenase enzyme itself [72]. Here we consider only the process of O_2 removal by increasing respiration. To calculate this indirect cost, the concentration of O_2 present in the cell needs to be estimated.

Since the time scale of O_2 concentration inside a cell is short, we have assumed a pseudo steady state inside the cell; the O_2 diffusion rate inside a cell is always balanced by the respiration rate [14], which can be expressed as

$$\rho_{\mathrm{CO}} F_{\mathrm{O_2}} = R_{\mathrm{D}}(\psi). \qquad (7)$$

Here ρ_{CO} is the conversion factor of respiratory O_2 to C equivalents and $F_{\mathrm{O_2}}$ is the actual O_2 diffusion rate into a cell from the particle and can be calculated as

$$F_{\mathrm{O_2}} = 4\pi r_{\mathrm{B}} K_{\mathrm{O_2}} \left(X_{\mathrm{O_2}} - X_{\mathrm{O_2,c}}\right), \quad (8)$$

where r_{B} is the cell radius, $X_{\mathrm{O_2}}$ is the local O_2 concentration inside the particle, $X_{O_2,\mathrm{c}}$ is the cellular O_2 concentration, and $K_{\mathrm{O_2}}$ is the effective diffusion coefficient of O_2 over cell membrane layers. The effective diffusion coefficient can be calculated according to Inomura et al.[14] in terms of diffusion coefficient inside particles ($\overline{D}_{\mathrm{O_2}}$), the diffusivity of cell membrane layers relative to water (ε_{m}), the radius of cellular cytoplasm (r_{C}), and the thickness of cell membrane layers (L_{m}) as

$$K_{\mathrm{O_2}} = \overline{D}_{\mathrm{O_2}} \frac{\varepsilon_{\mathrm{m}}(r_{\mathrm{C}} + L_{\mathrm{m}})}{\varepsilon_{\mathrm{m}} r_{\mathrm{C}} + L_{\mathrm{m}}}. \qquad (9)$$

The apparent diffusivity inside particles ($\overline{D}_{\mathrm{O_2}}$) is considered as a fraction $f_{\mathrm{O_2}}$ of the diffusion coefficient in seawater ($D_{\mathrm{O_2}}$)

$$\overline{D}_{\mathrm{O_2}} = f_{\mathrm{O_2}} D_{\mathrm{O_2}}. \qquad (10)$$

Combining (7) and (8) gives the cellular O_2 concentration $X_{O_2,\mathrm{c}}$ as

$$X_{\mathrm{O_2,c}} = \max\left[0, X_{\mathrm{O_2}} - \frac{R_{\mathrm{D}}(\psi)}{4\pi r_{\mathrm{B}} K_{\mathrm{O_2}} \rho_{\mathrm{CO}}}\right]. \qquad (11)$$

If there is excess O_2 present in the cell after respiration ($X_{O_2,\mathrm{c}} > 0$), then the indirect cost of removing the excess O_2 to be able to perform N_2 fixation can be written as

$$R_{\mathrm{O}_2}(\psi) = H(\psi)\rho_{\mathrm{CO}} 4\pi r_{\mathrm{B}} K_{\mathrm{O}_2} X_{O_2,\mathrm{c}}, \quad (12)$$

where $H(\psi)$ is the Heaviside function:

$$H(\psi) = \begin{cases} 0, & \text{if } \psi = 0 \\ 1, & \text{if } \psi > 0 \end{cases}. \quad (13)$$

Therefore, the total aerobic respiratory cost becomes:

$$R_{\mathrm{tot,A}}(\psi) = R_{\mathrm{D}}(\psi) + R_{O_2}(\psi). \quad (14)$$

Case 2: Anaerobic respiration

When available O_2 is insufficient to maintain aerobic respiration ($R_{\mathrm{tot}}(\psi) > \rho_{\mathrm{CO}} F_{\mathrm{O}_2,\mathrm{max}}$), cells use NO_3^- and SO_4^{2-} for respiration. The potential NO_3^- uptake, $J_{\mathrm{NO}_3,\mathrm{pot}}$, is

$$J_{\mathrm{NO}_3,\mathrm{pot}} = M_{NO_3} \frac{A_{NO_3} X_{NO_3}}{A_{NO_3} X_{NO_3} + M_{NO_3}}, \quad (15)$$

where M_{NO_3} and A_{NO_3} are maximum uptake rate and affinity for NO_3^- uptake, respectively. However, the actual rate of NO_3^- uptake, J_{NO_3}, is determined by cellular respiration and can be written as

$$J_{\mathrm{NO}_3} = \min\left(J_{\mathrm{NO}_3,\mathrm{pot}}, \max\left(0, \frac{R_{\mathrm{tot,A}}(\psi) - \rho_{\mathrm{CO}} F_{\mathrm{O}_2,\mathrm{max}}}{\rho_{\mathrm{CNO}_3}}\right)\right), \quad (16)$$

where ρ_{CNO_3} is the conversion factor of respiratory NO_3^- to C equivalents and the maximum O_2 diffusion rate into a cell $F_{\mathrm{O}_2,\mathrm{max}}$ can be obtained by making cellular O_2 concentration $X_{O_2,\mathrm{c}}$ zero in (8) as

$$F_{\mathrm{O}_2,\mathrm{max}} = 4\pi r_{\mathrm{B}} K_{\mathrm{O}_2} X_{\mathrm{O}_2}, \quad (17)$$

Further, in the absence of sufficient NO_3^-, the cell uses SO_4^{2-} as an electron acceptor for respiration. Since the average concentration of SO_4^{2-} in seawater is 29 mmol L^{-1} [38], SO_4^{2-} is a non-

limiting nutrient for cell growth and the potential uptake rate of SO_4^{2-} is mainly governed by the maximum uptake rate as

$$J_{SO_4,pot} = M_{SO_4}, \quad (18)$$

where M_{SO_4} is the maximum uptake rate for SO_4^{2-} uptake. The actual rate of SO_4^{2-} uptake, J_{SO_4}, can be written as

$$J_{SO_4} = \min\left(J_{SO_4,pot}, \max\left(0, \frac{R_{tot,A}(\psi) - \rho_{CO}F_{O_2,max} - \rho_{CNO_3}F_{NO_3,pot}}{\rho_{CSO_4}}\right)\right), \quad (19)$$

where ρ_{CSO_4} is the conversion factor of respiratory SO_4^{2-} to C equivalents.

According to formulations (16) and (19), NO_3^- and SO_4^{2-} uptake occurs only when the diffusive flux of O_2, and both O_2 and NO_3^- are insufficient to maintain respiration. Moreover, the uptake rates of NO_3^- and SO_4^{2-} are regulated according to the cells' requirements.

Uptakes of NO_3^- and SO_4^{2-} incur extra metabolic costs $R_{NO_3}\rho_{CNO_3}J_{NO_3}$ and $R_{SO_4}\rho_{CSO_4}J_{SO_4}$, where R_{NO_3} and R_{SO_4} are costs per unit of NO_3^- and SO_4^{2-} uptake. The total respiratory cost can be written as

$$R_{tot}(\psi) = R_{tot,A}(\psi) + R_{NO_3}\rho_{CNO_3}J_{NO_3} + R_{SO_4}\rho_{CSO_4}J_{SO_4}. \quad (20)$$

Synthesis and growth rate

The assimilated C and N are combined to synthesize new structure. The synthesis rate is constrained by the limiting resource (Liebig's law of the minimum) and by available electron acceptors such that the total flux of C available for growth J_{tot} (μg C d^{-1}) is:

$$J_{tot}(\psi) = \min\left[J_C - R_{tot}(\psi),\ \rho_{CN,B}J_N(\psi),\ \rho_{CO}F_{O_2} + \rho_{CNO_3}J_{NO_3} + \rho_{CSO_4}J_{SO_4}\right]. \quad (21)$$

Here, the total available C for growth is $J_{\mathrm{C}} - R_{\mathrm{tot}}(\psi)$, the C required to synthesize biomass from N source is $\rho_{\mathrm{CN},B} J_N$, and the C equivalent inflow rate of electron acceptors to the cell is $\rho_{\mathrm{CO}} F_{O_2} + \rho_{\mathrm{CNO_3}} J_{\mathrm{NO_3}} + \rho_{\mathrm{CSO_4}} J_{\mathrm{SO_4}}$. We assume that excess C or N is released from the cell instantaneously.

Synthesis is not explicitly limited by a maximum synthesis capacity; synthesis is constrained by the C and N uptake in the functional responses (equations (28) and (29)). The division rate μ of the cell (d^{-1}) is the total flux of C available for growth divided by the C mass of the cell (x_B):

$$\mu(\psi) = J_{\mathrm{tot}}(\psi)/x_B. \quad (22)$$

The resulting division rate, μ, is a measure of the bacterial fitness and we assume that the cell regulates its N_2 fixation rate depending on the environmental conditions to gain additional N while maximizing its growth rate. The optimal value of the parameter regulating N_2 fixation ψ ($0 \leq \psi \leq 1$) then becomes:

$$\psi^* = \underset{\psi}{\mathrm{argmax}}\{\mu(\psi)\}, \quad (23)$$

and the corresponding optimal division rate becomes

$$\mu^* = \mu(\psi^*). \quad (24)$$

The particle model

We consider a sinking particle of radius r_P (cm) and volume V_P (cm^3) (Supplementary Fig. S1). The particle contains facultative nitrogen-fixing bacterial population $B(r)$ (cells L^{-1}), polysaccharides $C_{\mathrm{P}}(r)$ (µg G L^{-1}), and polypeptides $P_{\mathrm{P}}(r)$ (µg A L^{-1}) at a radial distance r (cm) from the center of the particle, where G and A stand for glucose and amino acids. We assume that only fractions f_{C} and f_{P} of these polymers are labile ($C_L(r) = f_{\mathrm{C}} C_{\mathrm{P}}(r), P_L(r) = f_{\mathrm{P}} P_{\mathrm{P}}(r)$), i.e.

accessible by bacteria. Bacterial enzymatic hydrolysis converts the labile polysaccharides and polypeptides into monosaccharides (glucose) (G μg G L^{-1}) and amino acids (A μg A L^{-1}) that are efficiently taken up by bacteria. Moreover, the particle contains O_2, NO_3^-, and SO_4^{2-} with concentrations $X_{O_2}(r)$ (μmol O_2 L^{-1}), $X_{NO_3}(r)$ (μmol NO_3 L^{-1}), and $X_{SO_4}(r)$ (μmol SO_4 L^{-1}). Glucose and amino acids diffuse out of the particle whereas O_2 and NO_3^- diffuse into the particle from the surrounding environment. Due to the high concentration of SO_4^{2-} in ocean waters, we assume that SO_4^{2-} is not diffusion limited inside particles, its uptake is limited by the maximum uptake capacity due to physical constraint. The interactions between particle, cells, and the surrounding environment are explained in Supplementary Fig. S1 and equations are provided in Table 1 of the main text.

We assume that labile polysaccharide (C_L) and polypeptide (P_L) are hydrolyzed into glucose and amino acids at rates J_C and J_P with the following functional form

$$J_C = h_C \frac{A_C C_L}{h_C + A_C C_L} \quad (26)$$

$$J_P = h_P \frac{A_P P_L}{h_P + A_P P_L} \quad (27)$$

where h_C and h_P are maximum hydrolysis rates of the carbohydrate and peptide pool, and A_C and A_P are respective affinities. J_G and J_A represent uptake of glucose and amino acids:

$$J_G = M_G \frac{A_G G}{A_G G + M_G} \quad (28)$$

$$J_A = M_A \frac{A_A A}{A_A A + M_A} \quad (29)$$

where M_G and M_A are maximum uptake rates of glucose and amino acids, whereas A_G and A_A are corresponding affinities. Hydrolyzed monomers diffuse out of the particle at a rate D_M.

546 μ^* is the optimal division rate of cells (equation (24)) and m_B represents the mortality rate of
547 bacteria. F_{O_2} and J_{NO_3} represent the diffusive flux of O_2 and the consumption rate of NO_3^-,
548 respectively, through the bacterial cell membrane. $\overline{D}_{O_2}$ and $\overline{D}_{NO_3}$ are diffusion coefficients of O_2
549 and NO_3^- inside the particle.

550 At the center of the particle ($r = 0$) the gradient of all quantities vanishes:

551 $$\left.\frac{\partial G}{\partial r}\right|_{r=0} = \left.\frac{\partial A}{\partial r}\right|_{r=0} = \left.\frac{\partial X_{O_2}}{\partial r}\right|_{r=0} = \left.\frac{\partial X_{NO_3}}{\partial r}\right|_{r=0} = 0 \quad (30)$$

552 At the surface of the particle ($r = r_P$) concentrations are determined by the surrounding
553 environment:

554 $$G|_{r=r_P} = G_\infty, A|_{r=r_P} = A_\infty, X_{O_2}\big|_{r=r_P} = X_{O_2,\infty},\ X_{NO_3}\big|_{r=r_P} = X_{NO_3,\infty}, \quad (31)$$

555 where G_∞, A_∞, $X_{O_2,\infty}$ and $X_{NO_3,\infty}$ are concentrations of glucose, amino acids, O_2, and NO_3^- in the
556 environment.

557 ***Calculation of total N_2 fixation rate***

558 The total amount of fixed N_2 in a specific size class of particle, $N_{fix,P}$ (μg N particle^{-1}), is calculated
559 as

560 $$N_{fix,P} = \int\int 4\pi {r_B}^2 B J_{N_2}\, dr_P\, dz, \qquad (32)$$

561 where r_P (cm) is the particle radius and z (m) represents the water column depth.

562 N_2 fixation rate per unit volume of water, $N_{fix,V}(t)$ (μmol N m^{-3} d^{-1}), is calculated as

$$\mathrm{N_{fix,V}} = \int\int 4\pi {r_B}^2 \rho B J_{\mathrm{N_2}} n(x) \mathrm{d}r_P \mathrm{d}x, \qquad (33)$$

Here x (cm) represents the size range (radius) of particles, ρ is the fraction of diazotrophs of the total heterotrophic bacteria, and $n(x)$ (number of particles per unit volume of water per size increment) is the size spectrum of particles that is most commonly approximated by a power law distribution of the form

$$n(x) = n_0 (2x)^{\xi}, \qquad (34)$$

where n_0 is a constant that controls total particle abundance and the slope ξ represents the relative concentration of small to large particles: the steeper the slope, the greater the proportion of smaller particles and the flatter the slope, and the greater the proportion of larger particles[35].

Depth-integrated N_2 fixation rate, $\mathrm{N_{fix,D}}$ (μmol N m^{-2} d^{-1}), can be obtained by

$$\mathrm{N_{fix,D}}(t) = \int \mathrm{N_{fix,V}} \mathrm{d}z. \qquad (35)$$

Assumptions and simplification in the modelling approach

According to our current model formulation, the particle size remains constant while sinking. However, in nature, particle size is dynamic due to processes like bacterial remineralization, aggregation, and disaggregation. We neglect these complications to keep the model simple and to focus on revealing the coupling between particle-associated environmental conditions and N_2 fixation by heterotrophic bacteria. These factors can, however, possibly be incorporated by using *in situ* data or by using the relationship between carbon content and the diameter of particles[46] and including terms for aggregation and disaggregation[53].

582 Our model represents a population of facultative heterotrophic diazotrophs that grow at a rate
583 similar to other heterotrophic bacteria but the whole community initiates N_2 fixation when
584 conditions become suitable. However, under natural conditions, diazotrophs may only constitute a
585 fraction of the bacterial community, and their proliferation may be gradual[20], presumably affected
586 by multiple factors. In such case, our approach will overestimate diazotroph cell concentration and
587 consequently the N_2 fixation rate.

588 For simplicity, our approach includes only aerobic respiration, NO_3^- and SO_4^{2-} respiration,
589 although many additional aerobic and anaerobic processes likely occur on particles (e.g Klawonn et
590 al.[18]). To our knowledge, a complete picture of such processes, their interactions and effects on
591 particle biochemistry is unavailable. For example, we have assumed that when O_2 and NO_3^- are
592 insufficient to maintain respiration, heterotrophic bacteria start reducing SO_4^{2-}. However, SO_4^{2-}
593 reduction has been detected only with a significant lag after the occurrence of anaerobic conditions,
594 suggesting it as a slow adapted process[74], whereas we assume it to be instantaneous. On the other
595 hand, the lag may not be real but due to a 'cryptic sulfur cycle', where SO_4^{2-} reduction is
596 accompanied by concurrent sulfide oxidation effectively masking sulfide production[75]. Hopefully,
597 future insights into interactions between diverse aerobic and anaerobic microbial processes can
598 refine our modelling approach and fine-tune predictions of biochemistry in marine particles.

599

600

601

602

603

References

1. Gruber, N. & Galloway, J. N. An Earth-system perspective of the global nitrogen cycle. *Nature* **451**, 293–296 (2008).

2. Karl, D. *et al.* Dinitrogen fixation in the world's oceans. in *The Nitrogen Cycle at Regional to Global Scales* 47–98 (Springer Netherlands, 2002). doi:10.1007/978-94-017-3405-9_2

3. Falkowski, P. G. Evolution of the nitrogen cycle and its influence on the biological sequestration of CO2 in the ocean. *Nature* **387**, 272–275 (1997).

4. Zehr, J. P. Nitrogen fixation by marine cyanobacteria. *Trends Microbiol.* **19**, 162–173 (2011).

5. Benavides, M., Bonnet, S., Berman-Frank, I. & Riemann, L. Deep into oceanic N2 fixation. *Front. Mar. Sci.* **5**, 108 (2018).

6. Mulholland, M. R. *et al.* High Rates of N2 Fixation in Temperate, Western North Atlantic Coastal Waters Expand the Realm of Marine Diazotrophy. *Global Biogeochem. Cycles* **33**, 826–840 (2019).

7. Blais, M. *et al.* Nitrogen fixation and identification of potential diazotrophs in the Canadian Arctic. *Global Biogeochem. Cycles* **26**, (2012).

8. Farnelid, H. *et al.* Nitrogenase gene amplicons from global marine surface waters are dominated by genes of non-cyanobacteria. *PLoS One* **6**, (2011).

9. Moisander, P. H. *et al.* Chasing after non-cyanobacterial nitrogen fixation in marine pelagic environments. *Front. Microbiol.* **8**, (2017).

624 10. Bombar, D., Paerl, R. W. & Riemann, L. Marine Non-Cyanobacterial Diazotrophs: Moving
625 beyond Molecular Detection. *Trends in Microbiology* **24**, 916–927 (2016).

626 11. Goldberg, I., Nadler, V. & Hochman, A. Mechanism of nitrogenase switch-off by oxygen. *J.*
627 *Bacteriol.* **169**, 874–879 (1987).

628 12. Fay, P. Oxygen relations of nitrogen fixation in cyanobacteria. *Microbiol. Rev.* **56**, 340–373
629 (1992).

630 13. Bentzon-Tilia, M., Severin, I., Hansen, L. H. & Riemann, L. Genomics and ecophysiology of
631 heterotrophic nitrogen-fixing bacteria isolated from estuarine surface water. *MBio* **6**, (2015).

632 14. Inomura, K., Bragg, J. & Follows, M. J. A quantitative analysis of the direct and indirect
633 costs of nitrogen fixation: A model based on Azotobacter vinelandii. *ISME J.* **11**, 166–175
634 (2017).

635 15. Paerl, H. W. & Prufert, L. E. Oxygen-poor microzones as potential sites of microbial N2
636 fixation in nitrogen-depleted aerobic marine waters. *Appl. Environ. Microbiol.* **53**, 1078–87
637 (1987).

638 16. Paerl, H. W. Microzone formation: Its role in the enhancement of aquatic N2 fixation.
639 *Limnol. Oceanogr.* **30**, 1246–1252 (1985).

640 17. Riemann, L., Steward, G. F. & Azam, F. Dynamics of bacterial community composition and
641 activity during a mesocosm diatom bloom (Applied and Environmental Microbiology (2000)
642 66:2 (578-587)). *Appl. Environ. Microbiol.* **66**, 578–587 (2000).

643 18. Klawonn, I., Bonaglia, S., Brüchert, V. & Ploug, H. Aerobic and anaerobic nitrogen
644 transformation processes in N2-fixing cyanobacterial aggregates. *ISME J.* **9**, 1456–1466

(2015).

19. Ploug, H., Kühl, M., Buchholz-Cleven, B. & Jørgensen, B. B. Anoxic aggregates - An ephemeral phenomenon in the pelagic environment? *Aquat. Microb. Ecol.* **13**, 285–294 (1997).

20. Pedersen, J. N., Bombar, D., Paerl, R. W. & Riemann, L. Diazotrophs and N2-Fixation associated with particles in coastal estuarine waters. *Front. Microbiol.* **9**, 1–11 (2018).

21. Rahav, E., Giannetto, M. J. & Bar-Zeev, E. Contribution of mono and polysaccharides to heterotrophic N2 fixation at the eastern Mediterranean coastline. *Sci. Rep.* **6**, 1–11 (2016).

22. Scavotto, R. E., Dziallas, C., Bentzon-Tilia, M., Riemann, L. & Moisander, P. H. Nitrogen-fixing bacteria associated with copepods in coastal waters of the North Atlantic Ocean. *Environ. Microbiol.* **17**, 3754–3765 (2015).

23. Yang, Q. S. *et al.* Analysis of nifH DNA and RNA reveals a disproportionate contribution to nitrogenase activities by rare plankton-associated diazotrophs. *BMC Microbiol.* **19**, 188 (2019).

24. Farnelid, H. *et al.* Diverse diazotrophs are present on sinking particles in the North Pacific Subtropical Gyre. *ISME J.* **13**, 170–182 (2019).

25. Geisler, E., Bogler, A., Rahav, E. & Bar-Zeev, E. Direct Detection of Heterotrophic Diazotrophs Associated with Planktonic Aggregates. *Sci. Rep.* **9**, 1–9 (2019).

26. Smith, D. C., Simon, M., Alldredge, A. L. & Azam, F. Intense hydrolytic enzyme activity on marine aggregates and implications for rapid particle dissolution. *Nature* **359**, 139–142 (1992).

27. Ploug, H. & Bergkvist, J. Oxygen diffusion limitation and ammonium production within sinking diatom aggregates under hypoxic and anoxic conditions. *Mar. Chem.* **176**, 142–149 (2015).

28. Gunsalus, R. P. Control of electron flow in Escherichia coli: Coordinated transcription of respiratory pathway genes. *Journal of Bacteriology* **174**, 7069–7074 (1992).

29. Kirchman, D. L. *Processes in Microbial Ecology*. (Oxford University Press, 2012).

30. Riederer-Henderson, M. A. & Wilson, P. W. Nitrogen fixation by sulphate-reducing bacteria. *J. Gen. Microbiol.* **61**, 27–31 (1970).

31. Postgate, J. R. & Kent, H. M. Diazotrophy within Desulfovibrio. *J. Gen. Microbiol.* **131**, 2119–2122 (1985).

32. Bertics, V. J. *et al.* Occurrence of benthic microbial nitrogen fixation coupled to sulfate reduction in the seasonally hypoxic Eckernförde Bay, Baltic Sea. *Biogeosciences* **10**, 1243–1258 (2013).

33. Steppe, T. F. & Paerl, H. W. Potential N2 fixation by sulfate-reducing bacteria in a marine intertidal microbial mat. *Aquat. Microb. Ecol.* **28**, 1–12 (2002).

34. McDonnell, A. M. P. & Buesseler, K. O. Variability in the average sinking velocity of marine particles. *Limnol. Oceanogr.* **55**, 2085–2096 (2010).

35. Jackson, G. A. *et al.* Particle size spectra between 1 μm and 1 cm at Monterey Bay determined using multiple instruments. *Deep. Res. Part I Oceanogr. Res. Pap.* **44**, 1739–1767 (1997).

686 36. Jouandet, M.-P. *et al.* Optical imaging of mesopelagic particles indicates deep carbon flux
687 beneath a natural iron-fertilized bloom in the Southern Ocean. *Limnol. Oceanogr.* **56**, 1130–
688 1140 (2011).

689 37. Froelich, P. N. *et al.* Early oxidation of organic matter in pelagic sediments of the eastern
690 quatorial Atlantic: suboxic diagenesis. *Geochim. Cosmochim. Acta* **43**, 1075–1090 (1979).

691 38. Millero, F. J. *Chemical Oceanography*. (CRC Press, 2005).

692 39. Maun, M. *The Biology of Coastal Sand Dunes*. (Oxford University Press, 2009).

693 40. de Vicente, I., Ortega-Retuerta, E., Romera, O., Morales-Baquero, R. & Reche, I.
694 Contribution of transparent exopolymer particles to carbon sinking flux in an oligotrophic
695 reservoir. *Biogeochemistry* **96**, 13–23 (2009).

696 41. Friedrich, U., Schallenberg, M. & Holliger, C. Pelagic bacteria-particle interactions and
697 community-specific growth rates in four lakes along a trophic gradient. *Microb. Ecol.* **37**,
698 49–61 (1999).

699 42. Busch, K. *et al.* Bacterial colonization and vertical distribution of marine gel particles (TEP
700 and CSP) in the arctic Fram Strait. *Front. Mar. Sci.* **4**, 166 (2017).

701 43. Geisler, E., Bogler, A., Bar-Zeev, E. & Rahav, E. Heterotrophic Nitrogen Fixation at the
702 Hyper-Eutrophic Qishon River and Estuary System. *Front. Microbiol.* **11**, 2012–2021
703 (2020).

704 44. Kiøorboe, T. Formation and fate of marine snow: Small-scale processes with large-scale
705 implications. *Sci. Mar.* **65**, 57–71 (2001).

706 45. Martiny, A. C., Vrugt, J. A., Primeau, F. W. & Lomas, M. W. Regional variation in the
707 particulate organic carbon to nitrogen ratio in the surface ocean. *Global Biogeochem. Cycles*
708 **27**, 723–731 (2013).

709 46. Guidi, L. *et al.* Relationship between particle size distribution and flux in the mesopelagic
710 zone. *Deep. Res. Part I Oceanogr. Res. Pap.* **55**, 1364–1374 (2008).

711 47. Boström, K. H., Riemann, L., Kühl, M. & Hagström, Å. Isolation and gene quantification of
712 heterotrophic N2-fixing bacterioplankton in the Baltic Sea. *Environ. Microbiol.* **9**, 152–164
713 (2007).

714 48. Iversen, M. H. & Ploug, H. Ballast minerals and the sinking carbon flux in the ocean:
715 Carbon-specific respiration rates and sinking velocity of marine snow aggregates.
716 *Biogeosciences* **7**, 2613–2624 (2010).

717 49. Eduardo Menschel, A. & González, H. E. Carbon and Calcium Carbonate Export Driven by
718 Appendicularian Faecal Pellets in the Humboldt Current System off Chile. *Sci. Rep.* **9**, 1–12
719 (2019).

720 50. Wiedmann, I., Reigstad, M., Marquardt, M., Vader, A. & Gabrielsen, T. M. Seasonality of
721 vertical flux and sinking particle characteristics in an ice-free high arctic fjord-Different from
722 subarctic fjords? *J. Mar. Syst.* **154**, 192–205 (2016).

723 51. Bach, L. T. *et al.* The Influence of Plankton Community Structure on Sinking Velocity and
724 Remineralization Rate of Marine Aggregates. *Global Biogeochem. Cycles* **33**, 971–994
725 (2019).

726 52. Cram, J. A. *et al.* The Role of Particle Size, Ballast, Temperature, and Oxygen in the Sinking

727 Flux to the Deep Sea. *Global Biogeochem. Cycles* **32**, 858–876 (2018).

728 53. Bianchi, D., Weber, T. S., Kiko, R. & Deutsch, C. Global niche of marine anaerobic
729 metabolisms expanded by particle microenvironments. *Nat. Geosci.* **11**, 1–6 (2018).

730 54. Desai, M. S., Assig, K. & Dattagupta, S. Nitrogen fixation in distinct microbial niches within
731 a chemoautotrophy-driven cave ecosystem. *ISME J.* **7**, 2411–2423 (2013).

732 55. Leloup, J. *et al.* Sulfate-reducing bacteria in marine sediment (Aarhus Bay, Denmark):
733 Abundance and diversity related to geochemical zonation. *Environ. Microbiol.* **11**, 1278–
734 1291 (2009).

735 56. Berelson, W. M. Particle settling rates increase with depth in the ocean. *Deep. Res. Part II*
736 *Top. Stud. Oceanogr.* **49**, 237–251 (2001).

737 57. De La Rocha, C. L., Nowald, N. & Passow, U. Interactions between diatom aggregates,
738 minerals, particulate organic carbon, and dissolved organic matter: Further implications for
739 the ballast hypothesis. *Global Biogeochem. Cycles* **22**, (2008).

740 58. Ploug, H., Iversen, M. H. & Fischer, G. Ballast, sinking velocity, and apparent diffusivity
741 within marine snow and zooplankton fecal pellets: Implications for substrate turnover by
742 attached bacteria. *Limnol. Oceanogr.* **53**, 1878–1886 (2008).

743 59. Alldredge, A. L. & Gotschalk, C. In situ settling behavior of marine snow. *Limnol.*
744 *Oceanogr.* **33**, 339–351 (1988).

745 60. Garcia, H. *et al. World Ocean Atlas 2018, Volume 4: Dissolved Inorganic Nutrients*
746 *(phosphate, nitrate and nitrate+nitrite, silicate). A. Mishonov Technical Ed.; NOAA Atlas*
747 *NESDIS 84*. (2019).

748 61. Garcia, H. *et al. World Ocean Atlas 2018, Volume 3: Dissolved Oxygen, Apparent Oxygen*
749 *Utilization, and Oxygen Saturation. A. Mishonov Technical Ed.; NOAA Atlas NESDIS 83*.
750 (2019).

751 62. Wiedmann, I., Reigstad, M., Sundfjord, A. & Basedow, S. Potential drivers of sinking
752 particle's size spectra and vertical flux of particulate organic carbon (POC): Turbulence,
753 phytoplankton, and zooplankton. *J. Geophys. Res. Ocean.* **119**, 6900–6917 (2014).

754 63. Benavides, M. *et al.* Basin-wide N2 fixation in the deep waters of the Mediterranean Sea.
755 *Global Biogeochem. Cycles* **30**, 952–961 (2016).

756 64. Shiozaki, T., Ijichi, M., Kodama, T., Takeda, S. & Furuya, K. Heterotrophic bacteria as
757 major nitrogen fixers in the euphotic zone of the Indian Ocean. *Global Biogeochem. Cycles*
758 **28**, 1096–1110 (2014).

759 65. Halm, H. *et al.* Heterotrophic organisms dominate nitrogen fixation in the south pacific gyre.
760 *ISME J.* **6**, 1238–1249 (2012).

761 66. Luo, Y. W. *et al.* Database of diazotrophs in global ocean: Abundance, biomass and nitrogen
762 fixation rates. *Earth Syst. Sci. Data* **4**, 47–73 (2012).

763 67. Rahav, E. *et al.* Dinitrogen fixation in aphotic oxygenated marine environments. *Front.*
764 *Microbiol.* **4**, 227 (2013).

765 68. Boeuf, D. *et al.* Biological composition and microbial dynamics of sinking particulate
766 organic matter at abyssal depths in the oligotrophic open ocean. *Proc. Natl. Acad. Sci. U. S.*
767 *A.* **116**, 11824–11832 (2019).

768 69. Pirt, S. J. Maintenance energy: a general model for energy-limited and energy-sufficient

growth. *Arch. Microbiol.* **133**, 300–302 (1982).

70. Mislan, K. A. S., Stock, C. A., Dunne, J. P. & Sarmiento, J. L. Group behavior among model bacteria influences particulate carbon remineralization depths. *J. Mar. Res.* **72**, 183–218 (2014).

71. Dalton, H. & Postgate, J. R. Effect of Oxygen on Growth of Azotobacter chroococcum in Batch and Continuous Cultures. *J. Gen. Microbiol.* **54**, 463–473 (2009).

72. Oelze, J. Respiratory protection of nitrogenase in *Azotobacter* species: is a widely held hypothesis unequivocally supported by experimental evidence? *FEMS Microbiol. Rev.* **24**, 321–333 (2000).

73. Inomura, K., Bragg, J., Riemann, L. & Follows, M. J. A quantitative model of nitrogen fixation in the presence of ammonium. *PLoS One* **13**, e0208282 (2018).

74. Santegoeds, C. M., Ferdelman, T. G., Muyzer, G. & De Beer, D. Structural and functional dynamics of sulfate-reducing populations in bacterial biofilms. *Appl. Environ. Microbiol.* **64**, 3731–3739 (1998).

75. Callbeck, C. M. *et al.* Oxygen minimum zone cryptic sulfur cycling sustained by offshore transport of key sulfur oxidizing bacteria. *Nat. Commun.* **9**, 1–11 (2018).

76. Alldredge, A. L., Passow, U. & Haddock, S. H. D. The characteristics and transparent exopolymer particle (TEP) content of marine snow formed from thecate dinoflagellates. *J. Plankton Res.* **20**, 393–406 (1998).

Acknowledgments

SC and LR were supported by grant 6108-00013 from the Danish Council for Independent Research to LR. The Centre for Ocean Life was supported by the Villum Foundation. KI was supported by the Simons Foundation (Simons Postdoctoral Fellowship in Marine Microbial Ecology, Award 544338). MJF was supported by the Simons Collaboration on Computational Biogeochemical Modeling of Marine Ecosystems (CBIOMES; Simons Foundation grant no. 549931). We wish to thank Helle Ploug for her helpful comments on an earlier version of the manuscript.

Author contributions

SC, LR, KA, and AV developed the model. SC performed all numerical simulations and analyses with input from KA and AV. SC and LR wrote the manuscript. All authors provided critical feedback and helped shape the manuscript.

Competing interests

The authors declare no competing interests.

Figures:

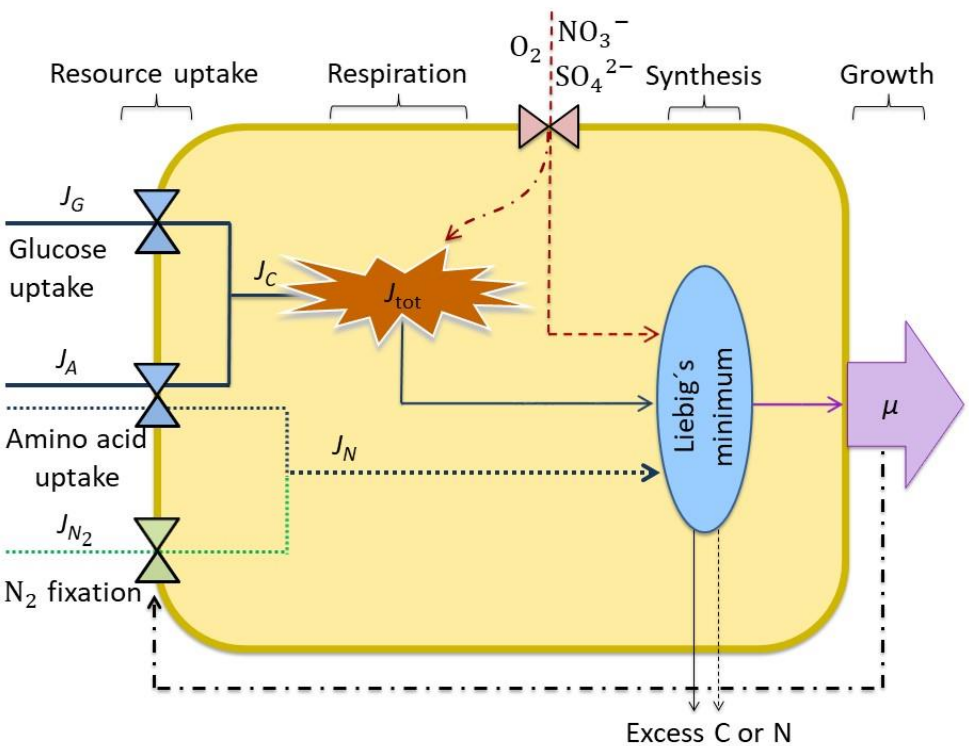

Fig. 1 Schematic representation of the cellular processes. It shows how fluxes of carbon (C), J_C (solid lines), fluxes of nitrogen (N), J_N (dotted lines), and electron acceptors (O_2, NO_3^-, and SO_4^{2-}; red dashed line) are combined (blue ellipse) to determine growth rate after paying the cost of respiration (brown explosion). Triangle symbols represent the functional responses for the uptake mechanisms and diffusive inflow of O_2, NO_3^-, and SO_4^{2-}. J_{tot} represents respiration that includes costs of uptake and mobilization of resources for synthesis, construction/maintenance of structure, and ectoenzyme production. The ellipse represents the synthesis of biomass from the available C, N and electron acceptors following Liebig's law of the minimum. Any excess assimilated C or N is excreted from the cell. μ represents the division rate. The black dashed-dotted line represents the regulation of N_2 fixation to optimize growth rate and the red dashed-dot line represents the regulation of respiration by electron acceptors.

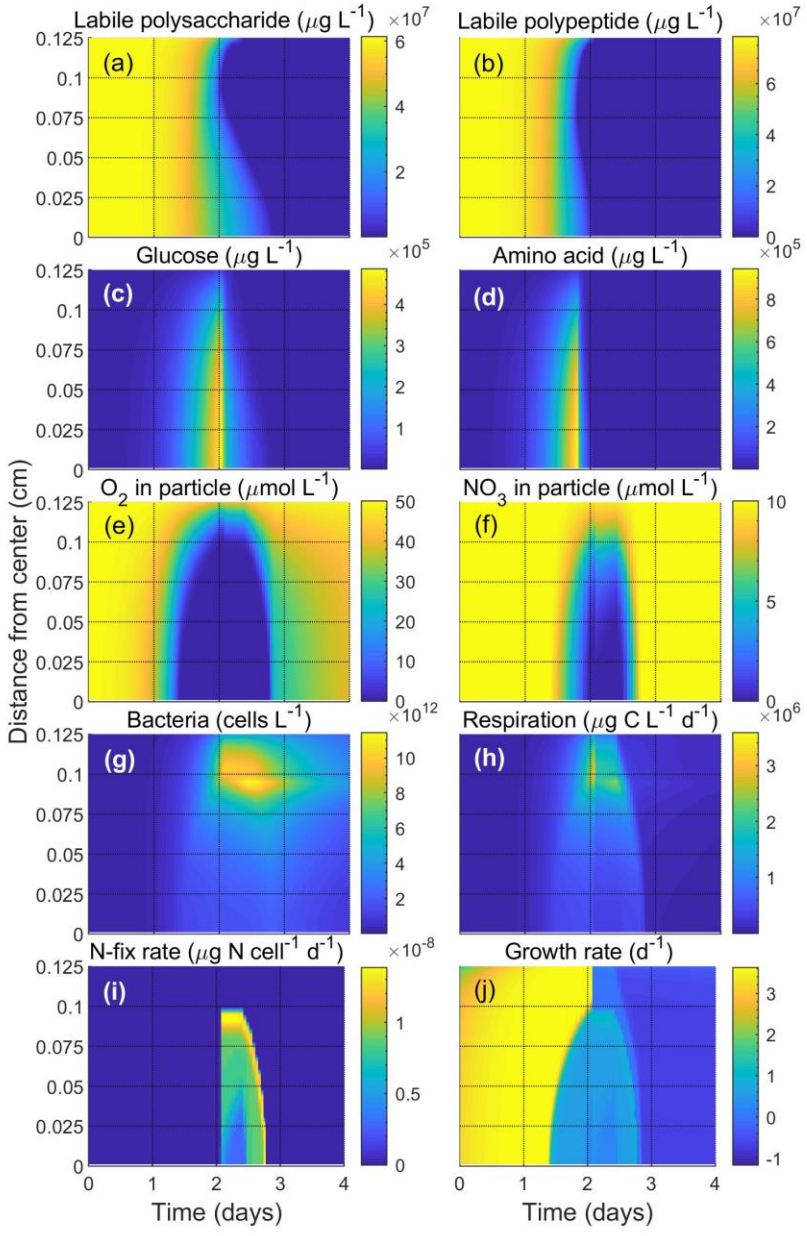

821

822 **Fig. 2** Dynamics inside a particle of radius 0.25 cm with time. (a) Labile carbohydrate, (b) labile
823 polypeptide, (c) glucose, (d) amino acid, (e) O_2 in particle, (f) NO_3^- in particle, (g) bacterial
824 abundance, (h) respiration rate, (i) N_2 fixation rate, and (j) growth rate are shown along the particle
825 radius over time. Parameters and concentrations of surrounding factors are taken from Table 2.

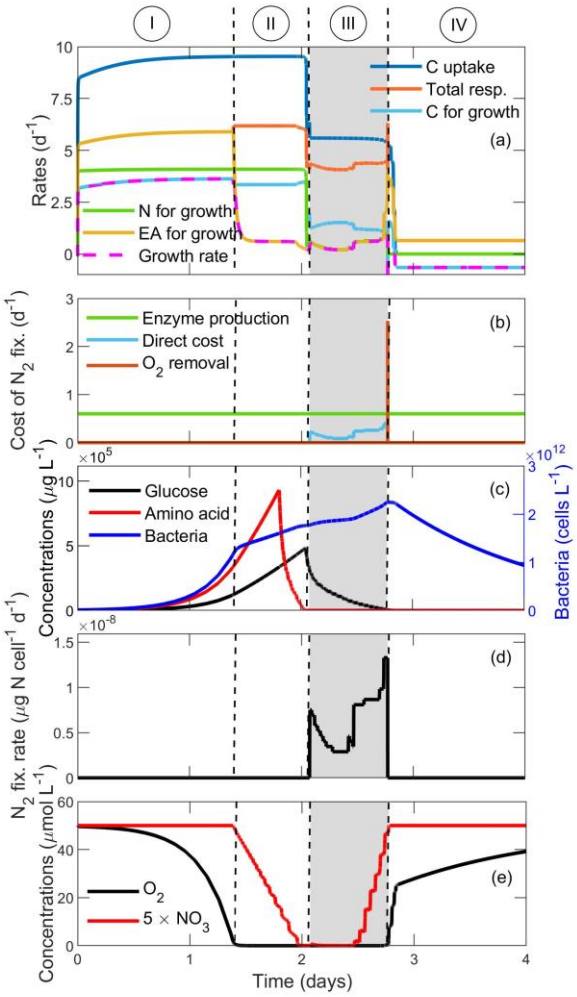

826

827 **Fig. 3** Cellular rates and resource concentrations at a radial distance of 0.027 cm from the center of
828 a 0.25 cm particle. (a) Size-specific rates of C uptake (dark blue), total respiration (orange),
829 available C for growth (light blue), available N for growth (green), available EA (electron acceptor
830 O_2, NO_3^-, and SO_4^{2-}; yellow), and growth rate of a cell (dashed magenta). Regions I, II, III, and IV
831 represent situations when a cell is limited by C, EA, co-limited by N and EA, N, and showing
832 negative growth rate (see text). (b) Respiratory costs related to N_2 fixation in terms of direct
833 respiration, enzyme production, and O_2 removal. (c) Glucose, amino acid, and bacterial
834 concentrations in the particle. (d) Cellular N_2 fixation rate. (e) O_2 and NO_3^- concentrations in the
835 particle. The grey area represents the time interval of N_2 fixation.

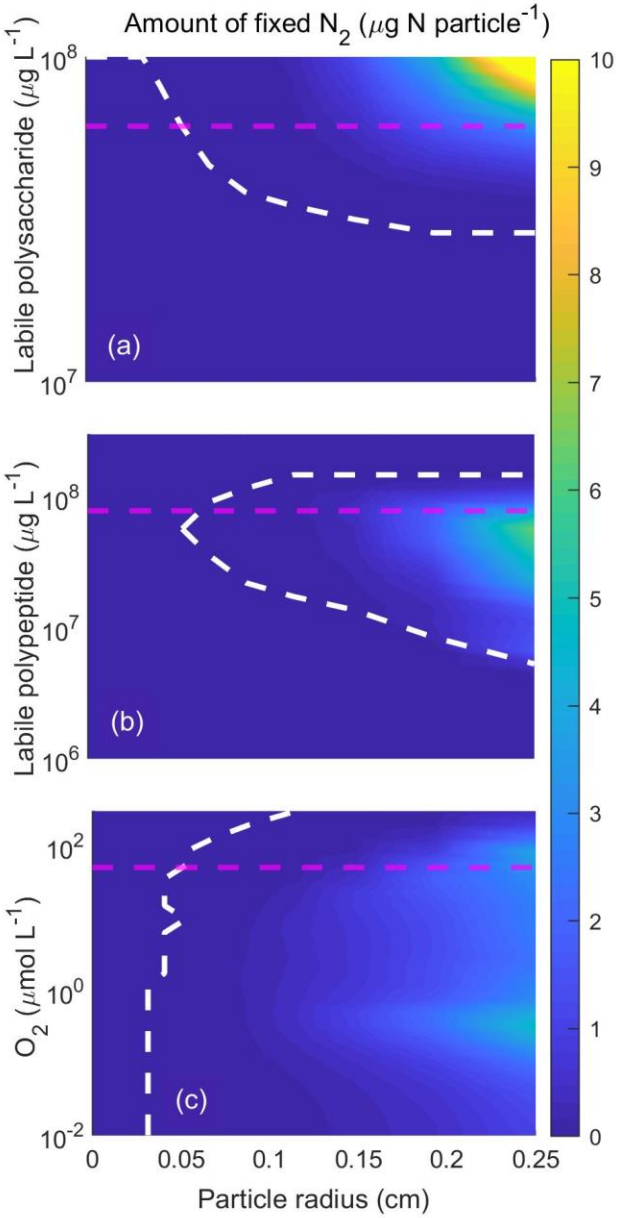

836

837 **Fig. 4** The total amount of fixed N_2 per particle as a function of particle radius and initial labile
838 polysaccharide (a), initial labile polypeptide (b), and surrounding O_2 concentration (c). The white
839 dashed line separates regions of occurrence and non-occurrence of N_2 fixation ($N_{fix} > 10^{-3}$ μg N
840 particle^{-1}). The horizontal magenta dashed lines indicate the base value for other plots, e.g., in (a),
841 magenta dashed line represents the level of polysaccharide concentration in panels b and c. The
842 chosen concentration ranges corresponds to those in natural particles [58,76].

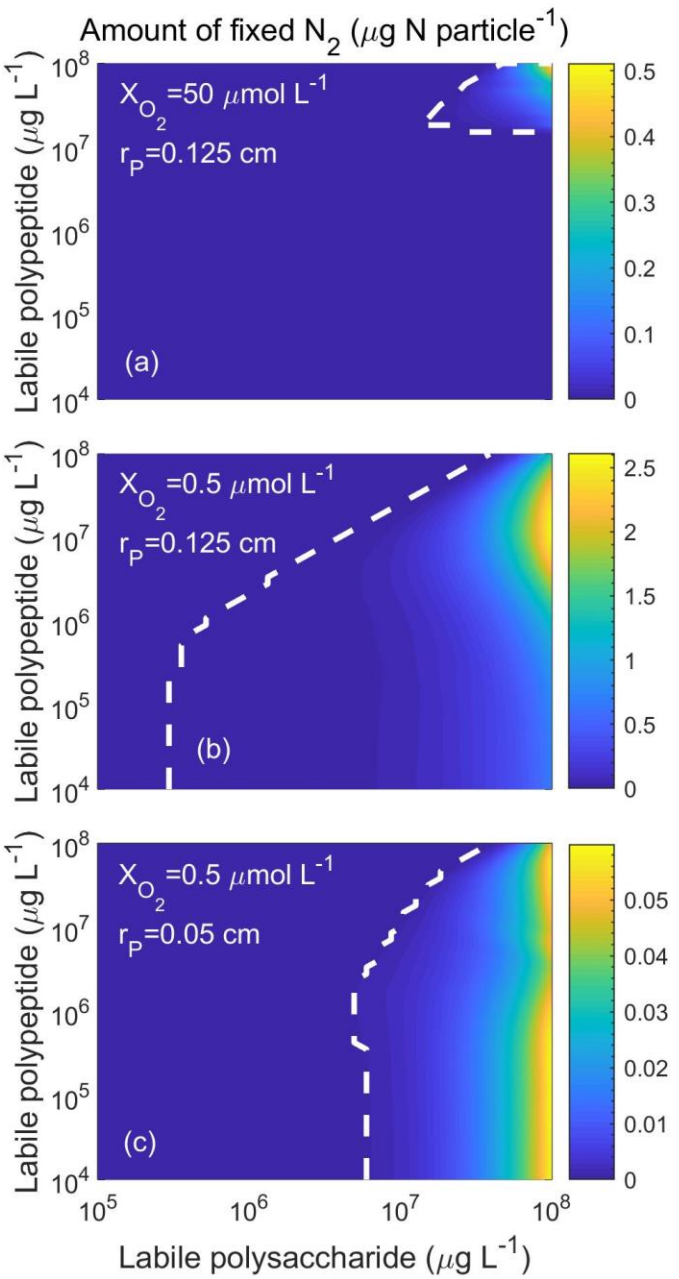

843

844 **Fig. 5** The total amount of fixed N_2 at different initial labile polysaccharide and polypeptide
845 concentrations. N_2 fixation is observed in a large particle of radius 0.125 cm and surrounding O_2
846 concentrations (a) 50 µmol O_2 L^{-1} and (b) 0.5 µmol O_2 L^{-1}, and (c) in a relatively smaller particle of
847 radius 0.05 cm and surrounding O_2 concentrations 0.5 µmol O_2 L^{-1}. Line types are similar as in Fig.
848 4. Note the different ranges of the scale of N2 fixation.

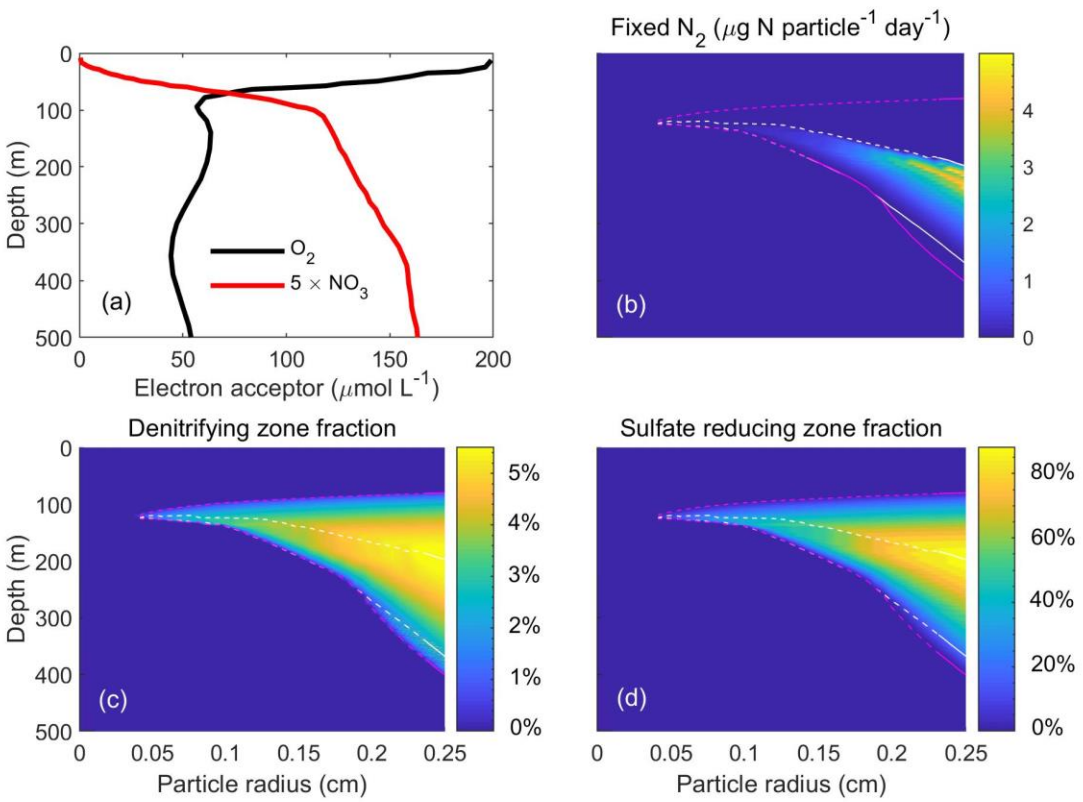

849

850 **Fig. 6** Dynamics inside sinking particles of different sizes in the upper 500 m of the water column.
851 (a) O_2 and NO_3^- profile in the water column [53]. Total amount of fixed N_2 per particle (b), fraction
852 of particle volume where respiration is fueled by denitrification (c), and fraction of particle volume
853 where respiration is fueled by SO_4^{2-} reduction (d). Areas enclosed by white and magenta dashed
854 lines represent the occurrence of N_2 fixation (>10^{-3} μg N day^{-1} particle^{-1}) and anoxia (O_2<10^{-3}
855 μmol O_2 L^{-1}), respectively, at the center of particles.

856

857

858

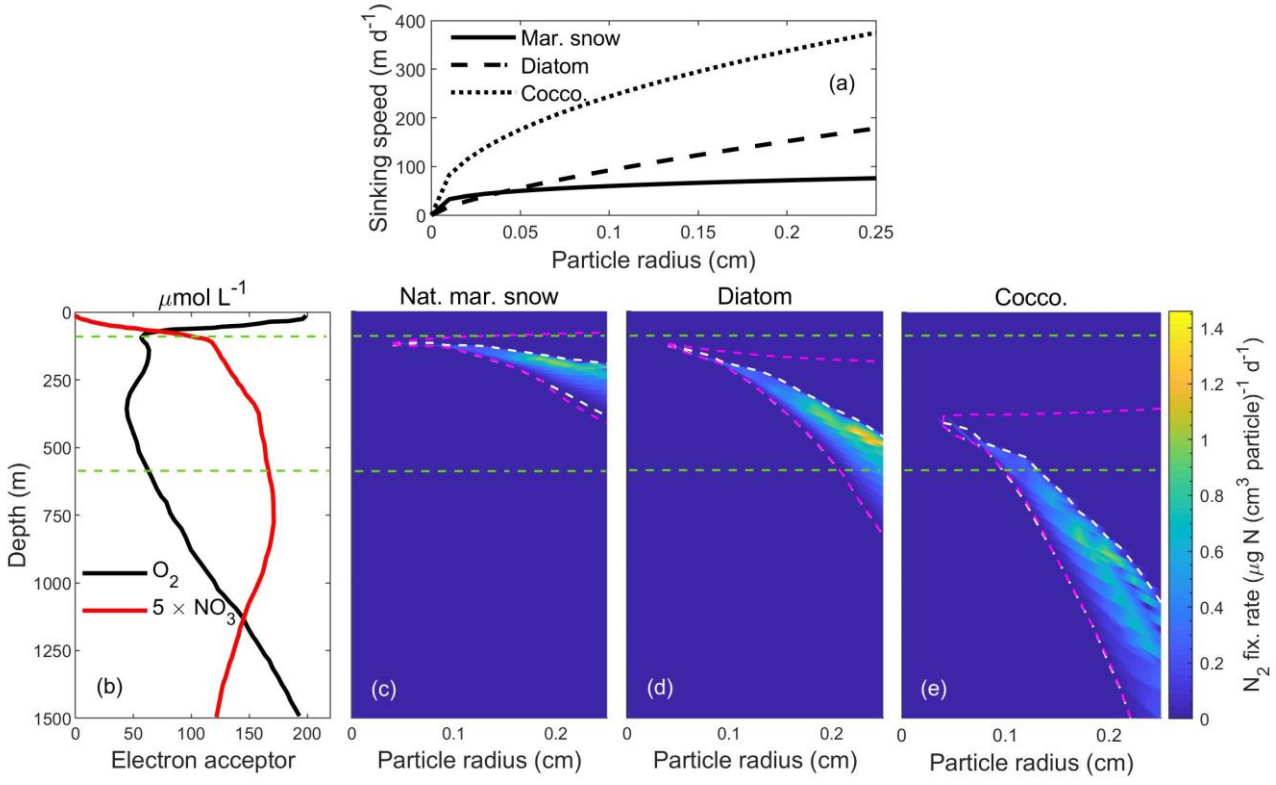

Fig. 7 N_2 fixation rates in different types of sinking particles with different sinking speeds. (a) Particle radius (cm) versus sinking speeds (m d^{-1}) of natural marine snow (continuous line) measured *in situ* off California ($v = 108.95 \times r_P^{0.26}$; [59]) and of laboratory-made diatom (dashed line) and coccolithophore (dotted line) aggregates measured *in vitro* ($v = 484.09 \times r_P^{0.72}$ and $v = 719.44 \times r_P^{0.47}$, respectively[48]). (b) O_2 and NO_3^- profiles in the water column[53]. (c-e) N_2 fixation rates per unit volume of particles of different sizes and types. White and magenta dashed lines are same as in Fig. 6. The area enclosed within the horizontal green lines represents the low-O_2 zone.

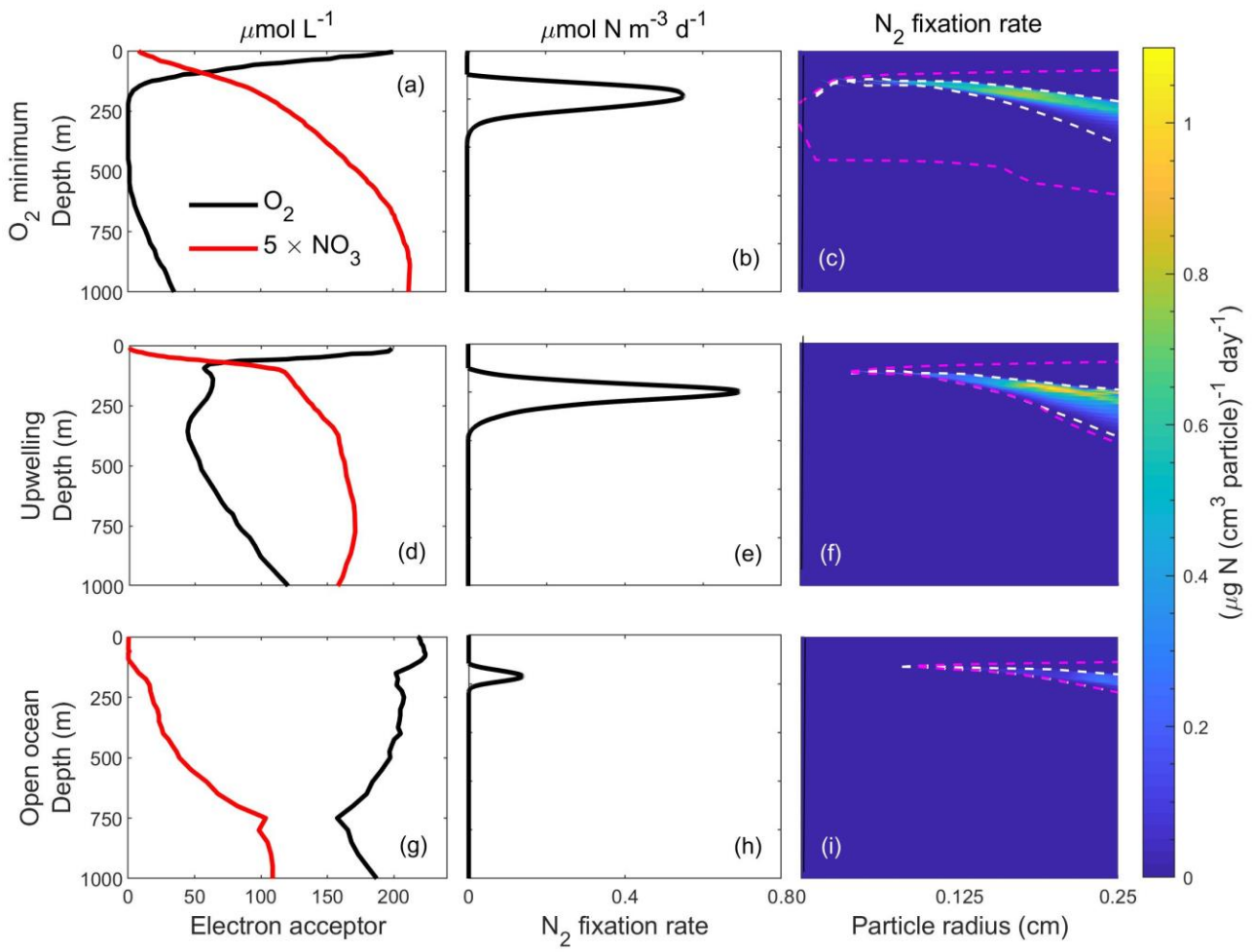

871

872 **Fig. 8** Comparison of predicted N_2 fixation rates in natural marine snow at three contrasting sites in
873 terms of vertical distributions of O_2 and NO_3 in the ocean: (a-c) O_2 minimum zone in the Eastern
874 Tropical South Pacific (ETSP)[53], (d-f) the Mauritanian upwelling zone in the North Atlantic Ocean
875 (NAO)[53], and (g-i) open ocean (OO; 30.5°N, 52.5°W)[60,61]. (a,d,g) O_2 and NO_3 concentrations in
876 the upper 1000 m vertical water column. (b,e,h) N_2 fixation rates per unit volume of water. (c,f,i) N_2
877 fixation rates per unit volume of particle of different size classes.

878

879

880

Table 1. Equations for the particle model. All quantities vary with time t and with distance from the center r. The operator in the brackets represents diffusion in spherical coordinates. Definitions, units, and values of each of the parameters are provided in Supplementary Table S1.

Variables	Equations	
Bacteria (cells L^{-1})	$\frac{\partial B}{\partial t} = \mu^*(G, A, X_{O_2}, X_{NO_3})B - m_B B$	25(a)
Labile polysaccharides (μg G L^{-1})	$\frac{\partial C_L}{\partial t} = -J_C B$	25(b)
Labile polypeptides (μg A L^{-1})	$\frac{\partial P_L}{\partial t} = -J_P B$	25(c)
Glucose (μg G L^{-1})	$\frac{\partial G}{\partial t} = J_C B - J_G B + D_M \left(\frac{\partial^2 G}{\partial r^2} + \frac{2}{r}\frac{\partial G}{\partial r}\right)$	25(d)
Amino acids (μg A L^{-1})	$\frac{\partial A}{\partial t} = J_P B - J_A B + D_M \left(\frac{\partial^2 A}{\partial r^2} + \frac{2}{r}\frac{\partial A}{\partial r}\right)$	25(e)
Oxygen (μmol O_2 L^{-1})	$\frac{\partial X_{O_2}}{\partial t} = -F_{O_2} B + \bar{D}_{O_2} \left(\frac{\partial^2 X_{O_2}}{\partial r^2} + \frac{2}{r}\frac{\partial X_{O_2}}{\partial r}\right)$	25(f)
Nitrate (μmol NO_3 L^{-1})	$\frac{\partial X_{NO_3}}{\partial t} = -J_{NO_3} B + \bar{D}_{NO_3} \left(\frac{\partial^2 X_{NO_3}}{\partial r^2} + \frac{2}{r}\frac{\partial X_{NO_3}}{\partial r}\right)$	25(g)

Figures

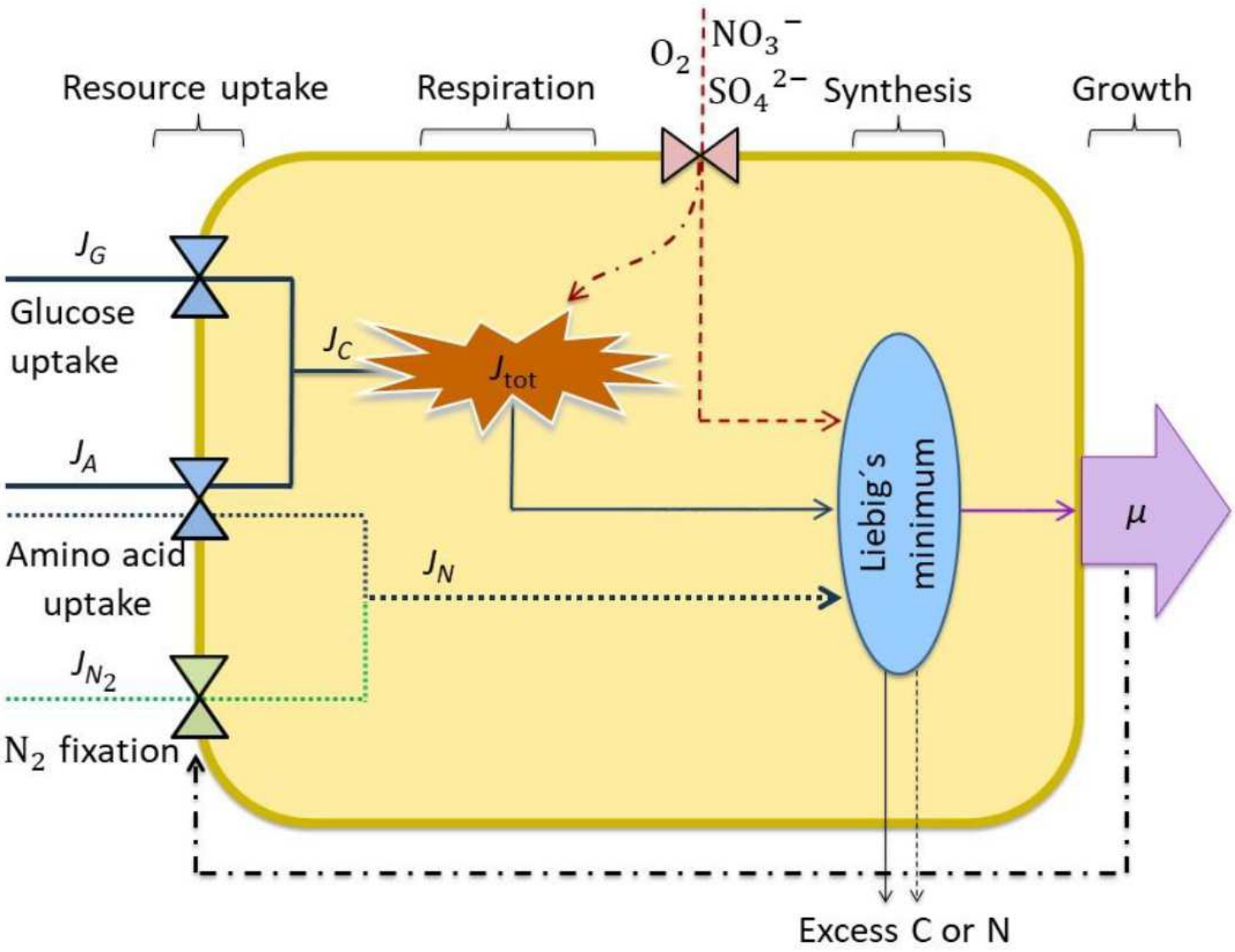

Figure 1

Schematic representation of the cellular processes. It shows how fluxes of carbon (C), C 811 (solid lines), fluxes of nitrogen (N), N (dotted lines), and electron acceptors (O2, NO3−, and SO42−; red dashed line) are combined (blue ellipse) to determine growth rate after paying the cost of respiration (brown explosion). Triangle symbols represent the functional responses for the uptake 814 mechanisms and diffusive inflow of O2, NO3−, and SO42−. tot represents respiration that in costs of uptake and mobilization of resources for synthesis, construction/maintenance of structure, and ectoenzyme production. The ellipse represents the synthesis of biomass from the available C, N and electron acceptors following Liebig's law of the minimum. Any excess assimilated C or N is excreted from the cell. μ represents the division rate. The black dashed-dotted line represents the regulation of N2 fixation to optimize growth rate and the red dashed-dot line represents the regulation of respiration by electron acceptors.

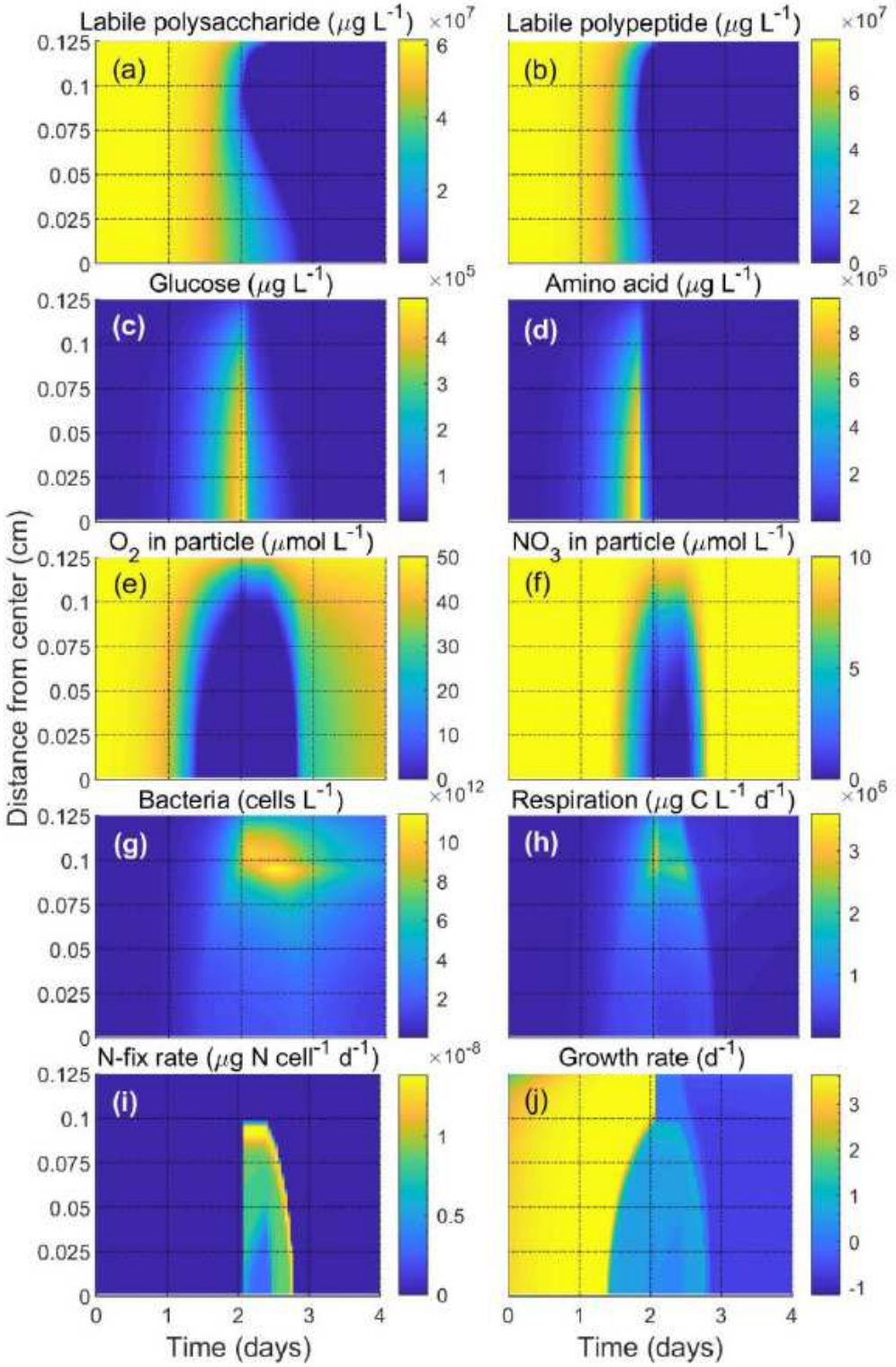

Figure 2

Dynamics inside a particle of radius 0.25 cm with time. (a) Labile carbohydrate, (b) labile polypeptide, (c) glucose, (d) amino acid, (e) O2 in particle, (f) NO3− in particle, (g) bacterial abundance, (h) respiration rate, (i) N2 fixation rate, and (j) growth rate are shown along the particle radius over time. Parameters and concentrations of surrounding factors are taken from Table 2.

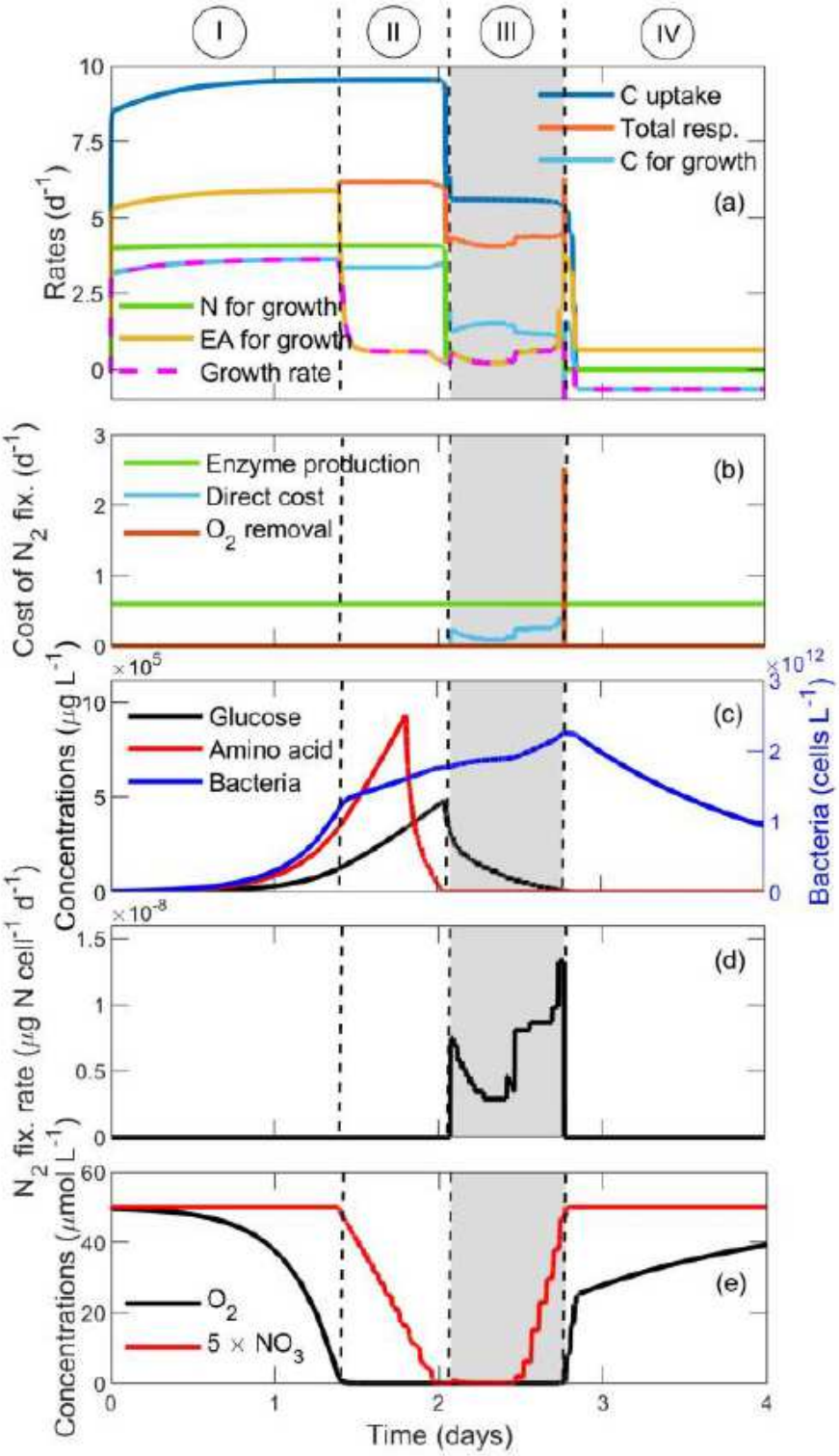

Figure 3

Cellular rates and resource concentrations at a radial distance of 0.027 cm from the center of a 0.25 cm particle. (a) Size-specific rates of C uptake (dark blue), total respiration (orange), available C for growth (light blue), available N for growth (green), available EA (electron acceptor 830 O2, NO3−, and SO42−; yellow), and growth rate of a cell (dashed magenta). Regions I, II, III, and IV represent situations when a cell is limited by C, EA, co-limited by N and EA, N, and showing negative growth rate (see text). (b)

Respiratory costs related to N2 fixation in terms of direct respiration, enzyme production, and O2 removal. (c) Glucose, amino acid, and bacterial concentrations in the particle. (d) Cellular N2 fixation rate. (e) O2 and NO3− concentrations in the particle. The grey area represents the time interval of N2 fixation.

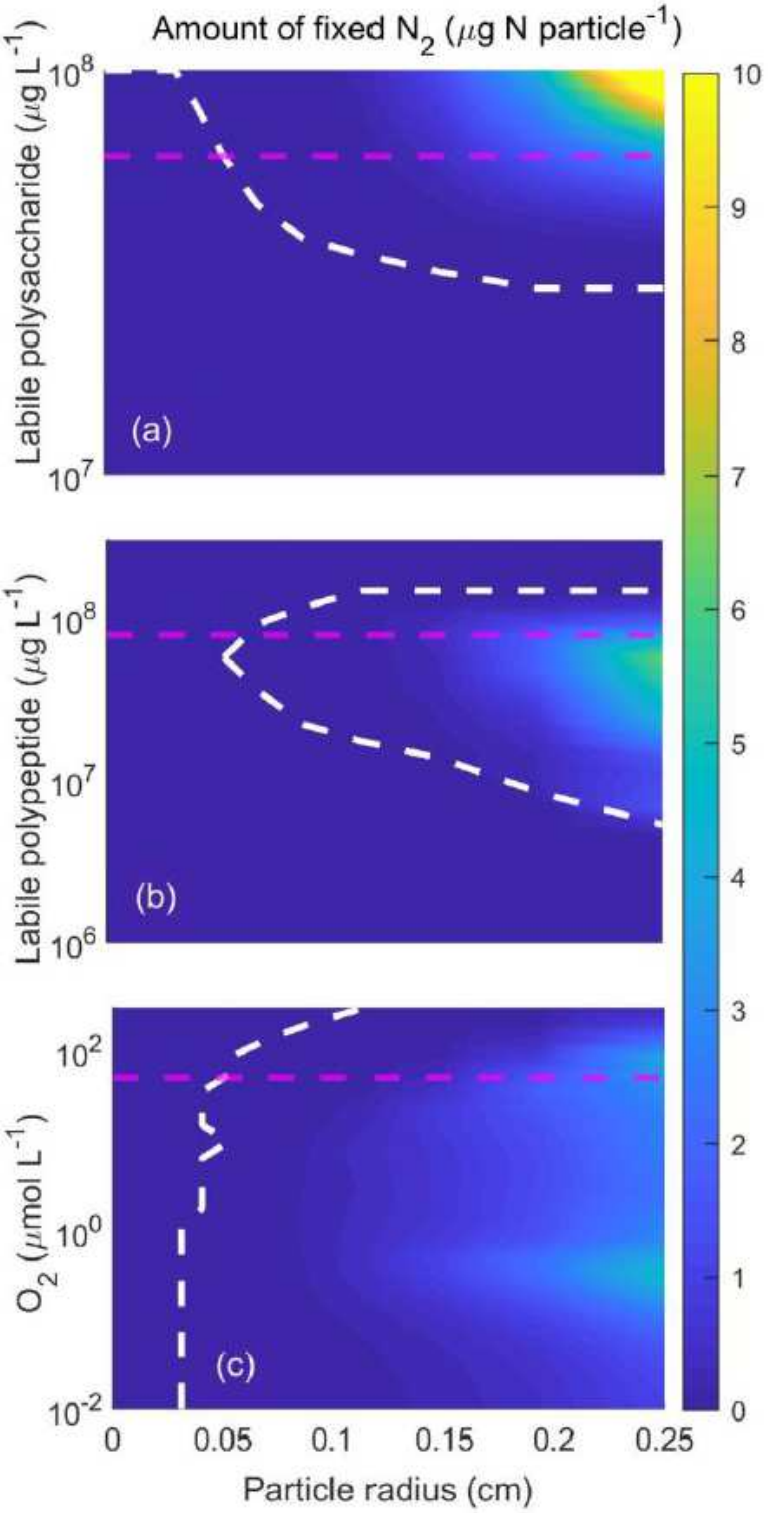

Figure 4

The total amount of fixed N2 per particle as a function of particle radius and initial labile polysaccharide (a), initial labile polypeptide (b), and surrounding O2 concentration (c). The white dashed line separates

regions of occurrence and non-occurrence of N2 fixation (Nfix > 10−3 µg N particle-1). The horizontal magenta dashed lines indicate the base value for other plots, e.g., in (a), magenta dashed line represents the level of polysaccharide concentration in panels b and c. The chosen concentration ranges corresponds to those in natural particles 58,76.

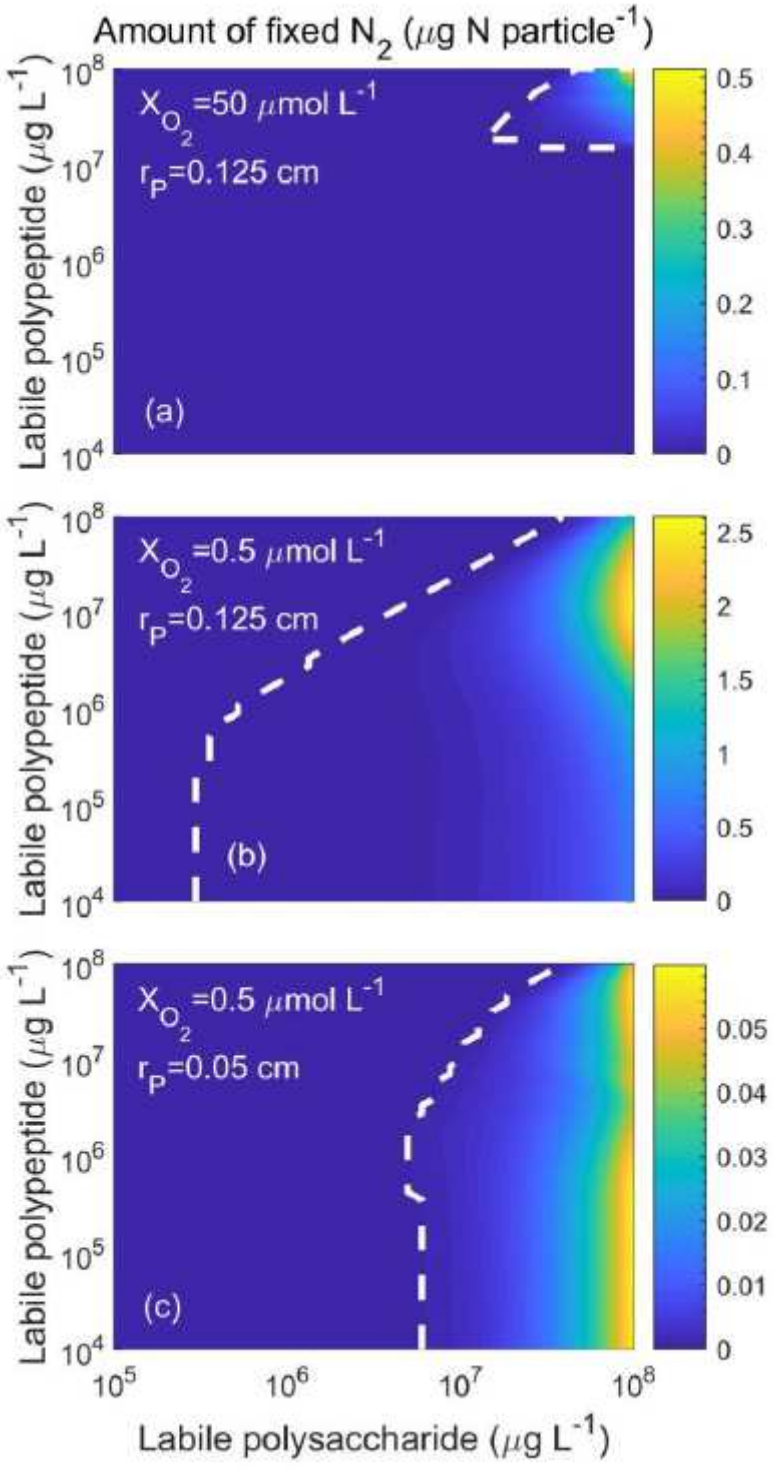

Figure 5

The total amount of fixed N2 at different initial labile polysaccharide and polypeptide concentrations. N2 fixation is observed in a large particle of radius 0.125 cm and surrounding O2 concentrations (a) 50 µmol

2 L-1 and (b) 0.5 µmol 2 L-1, and (c) in a relatively smaller particle of radius 0.05 cm and surrounding O2 concentrations 0.5 µmol 2 L-1. Line types are similar as in Fig. 4. Note the different ranges of the scale of N2 fixation.

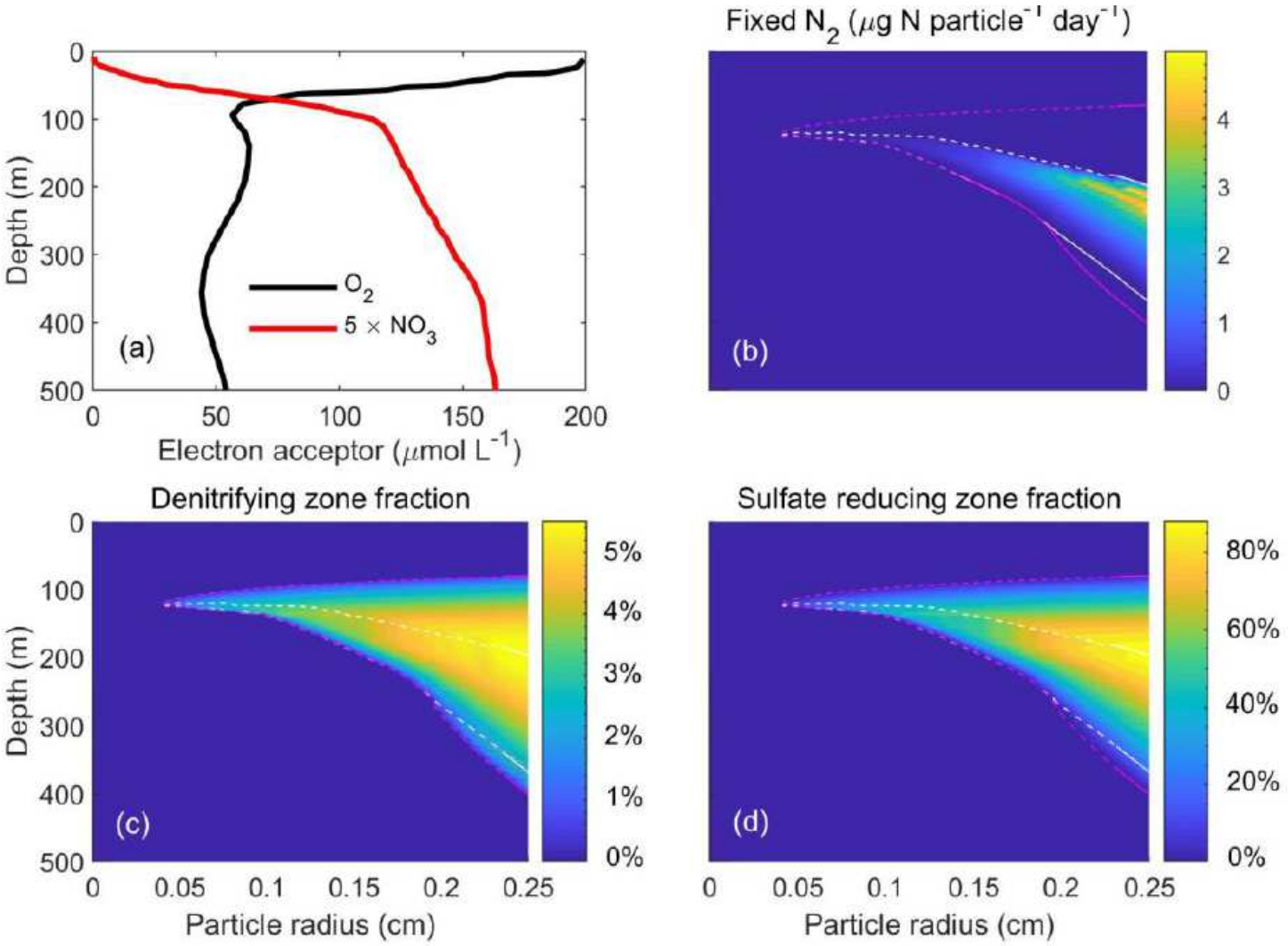

Figure 6

Dynamics inside sinking particles of different sizes in the upper 500 m of the water column. (a) O2 and NO3− profile in the water column 53. Total amount of fixed N2 per particle (b), fraction of particle volume where respiration is fueled by denitrification (c), and fraction of particle volume where respiration is fueled by SO42− reduction (d). Areas enclosed by white and magenta dashed lines represent the occurrence of N2 fixation (>10−3 µg N day-1 particle-1) and anoxia (O2<10−3 µmol 2 L-1), respectively, at the center of particles.

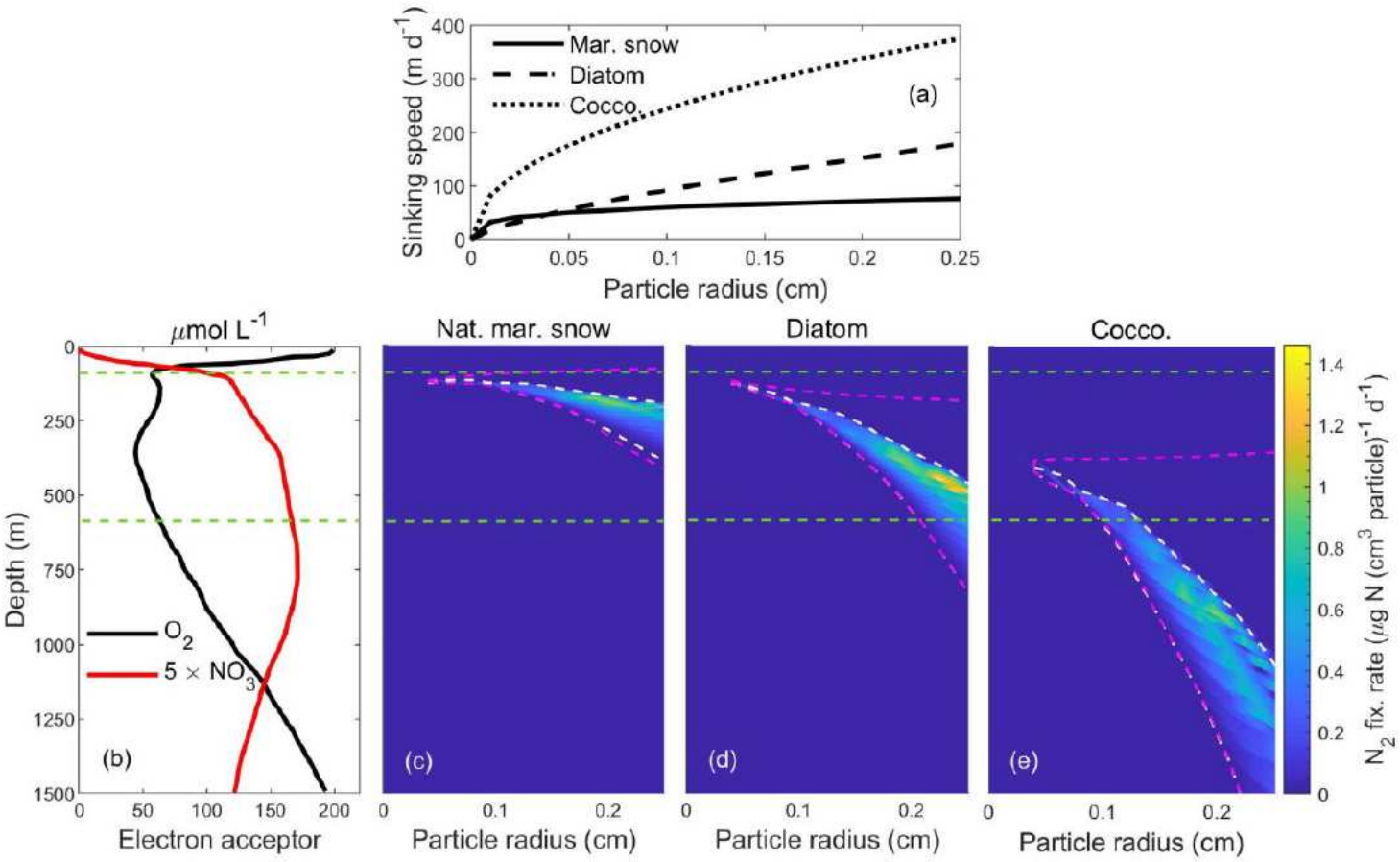

Figure 7

N2 fixation rates in different types of sinking particles with different sinking speeds. (a) Particle radius (cm) versus sinking speeds (m d-1) of natural marine snow (continuous line) measured in situ off California (= 108.95 × 0.26; 59) and of laboratory-made diatom (dashed line) and coccolithophore (dotted line) aggregates measured in vitro (= 484.09 × 0.72 and = 719.44 × 0.47, respectively48). (b) O2 and NO3− profiles in the water column53. (c-e) N2 fixation rates per unit volume of particles of different sizes and types. White and magenta dashed lines are same as in Fig. 6. The area enclosed within the horizontal green lines represents the low-O2 zone.

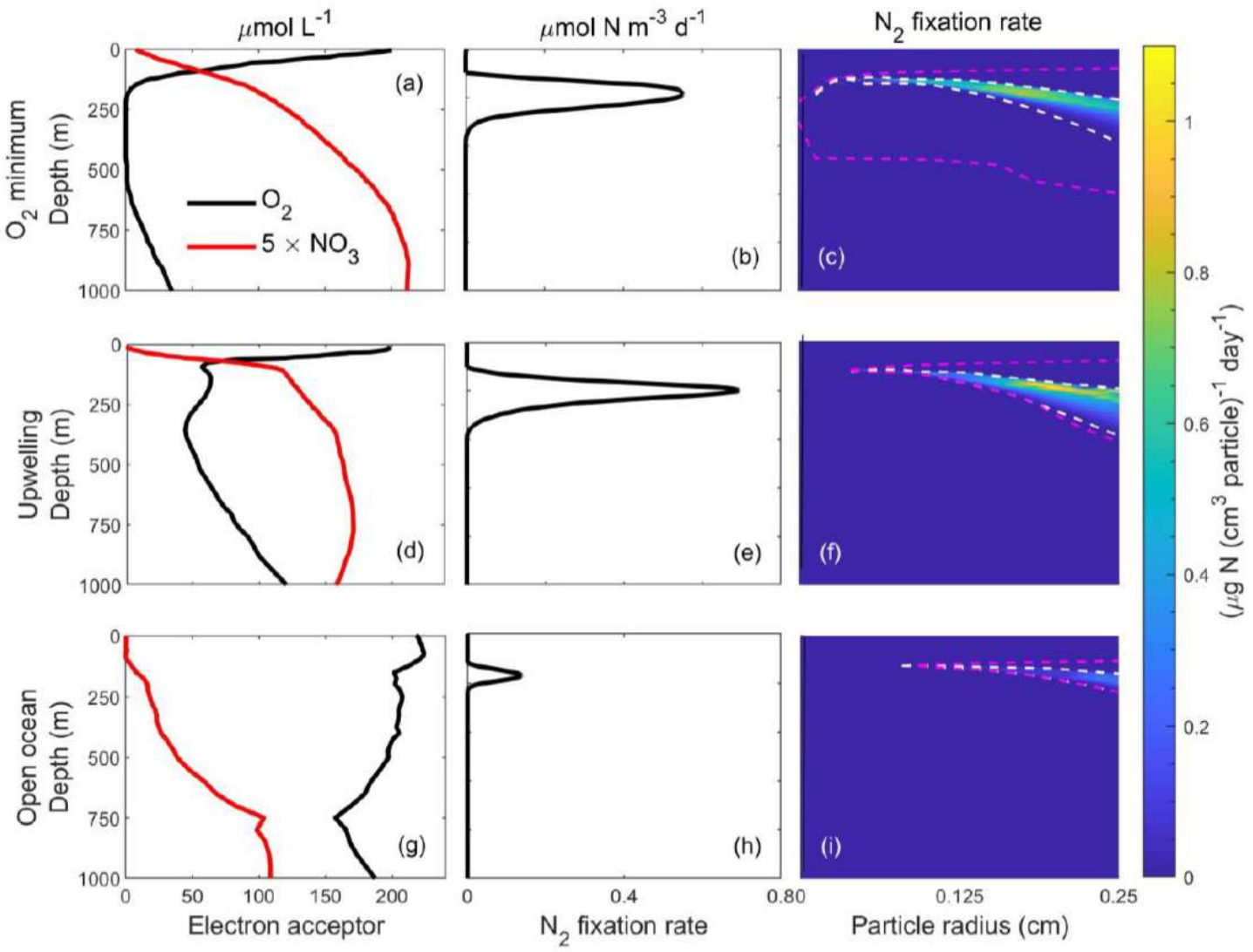

Figure 8

Comparison of predicted N2 fixation rates in natural marine snow at three contrasting sites in terms of vertical distributions of O2 and NO3 in the ocean: (a-c) O2 minimum zone in the Eastern Tropical South Pacific (ETSP)53, (d-f) the Mauritanian upwelling zone in the North Atlantic Ocean (NAO)53, and (g-i) open ocean (OO; 30.5oN, 52.5oW)60,61. (a,d,g) O2 and NO3 concentrations in the upper 1000 m vertical water column. (b,e,h) N2 fixation rates per unit volume of water. (c,f,i) N2 fixation rates per unit volume of particle of different size classes.

Supplementary Files

This is a list of supplementary files associated with this preprint. Click to download.

- SuppChakrabortyetal04112020.pdf